**Atmospheric
Chemistry
and Physics
Discussions**

# Bulk microphysical properties of semi transparent cirrus from AIRS: a six years global climatology and statistical analysis in synergy with CALIPSO and CloudSat

**A. Guignard[1], C. J. Stubenrauch[1], A. J. Baran[2], and R. Armante[1]**

[1]Laboratoire de Météorologie Dynamique, Ecole Polytechnique, UMR8539, Palaiseau, France
[2]Met Office, Fitzroy Road, Exeter, EX1 3PB, UK

Correspondence to: A. Guignard (anthony.guignard@lmd.polytechnique.fr)

**ACPD**

11, 24671–24725, 2011

**Bulk microphysical properties of semi transparent cirrus from AIRS**

A. Guignard et al.

Title Page

| Abstract | Introduction |
| Conclusions | References |
| Tables | Figures |

|◄ | ►|
◄ | ►

Back | Close

Full Screen / Esc

Printer-friendly Version

Interactive Discussion

## Abstract

This article presents a retrieval method and a statistical analysis of the bulk micropysical properties of semi-transparent ice clouds using the Atmospheric Infrared Sounder (AIRS). Global and long-term coverage provides information on the effective diameter ($D_e$) and habits of ice crystals in relation with their environment, ice water path (IWP) and temperature. The method relies on spectral absorption differences between 8 and 12 µm that depend on ice crystal properties. Using single scattering properties for column-like or aggregate-like ice crystals, the method is sensitive to $D_e$ of up to 85 µm and IWP of up to 120 g m$^{-2}$. Uncertainties due to the hypotheses on atmospheric parameters and ice crystal single scattering properties as well as horizontal heterogeneities have been demonstrated to be small. The behaviour of bulk microphysical properties as a function of temperature demonstrates that pure ice clouds only occur when $T_{cld} < 230$ K. On a global scale, these clouds represent practically 25 % of all high clouds and are mainly encountered in the mid-latitudes during winter and in the tropics. Colocated Radar-Lidar Geometrical Profiling (GEOPROF) data reveal an increase in the vertical extent of these cloud layers during mid-latitude winter but which does not significantly impact ice crystal characteristics. A comparative study with bulk microphysical properties from the TIROS-N Operational Vertical Sounder (TOVS) reveals improvements, especially for optically thin and thick semi-transparent ice clouds. Finally, we investigated parametrizations of $D_e$ as a function of IWP or Ice Water Content (IWC), which could be useful for modelling cirrus in General Circulation Models.

## 1 Introduction

High clouds (with cloud top pressure smaller than 440 hPa) cover about 30 % of the globe (Wylie and Menzel., 1999; Wylie et al., 2004; Chepfer et al., 2010; Stubenrauch et al., 2006, 2010) and therefore strongly influence the radiation budget of the Earth. Depending on the formation process of cirrus clouds (large-scale lifting, convection,

A. Guignard et al.

atmospheric waves (Ivanova et al., 2001; Stith et al., 2002; Boehm et al., 2003; Luo et al., 2004), one expects a resulting difference in their microphysical properties. These then influence the Earth's radiation budget. In General Circulation Models (GCM), $D_e$ is often parameterized as a function of IWC or cloud temperature (Mc Farlane et al., 1992;
5  Donner et al., 1997; Bony et al., 2001; Edwards et al., 2007). Cloud optical properties are then calculated from the GCM diagnosed $D_e$, assuming a dominant ice crystal shape. Most such relationships are based on data from only a few places on Earth and for very limited time periods (Heymsfield et al., 1984; Korolev et al., 2001; Boudala et al., 2002; Mc Farquhar et al., 2003; Garrett et al., 2004), and are also likely to be
10  affected by ice crystal shattering (Korolev et al., 2004; Field et al., 2006; Mc Farquhar et al., 2007). Even if satellite observations only allow us to retrieve bulk microphysical properties and rely on various assumptions, they provide a unique possibility to study correlations over the whole globe.

Compared to other passive remote sensing instruments, the high spectral resolu-
15  tion infrared (IR) vertical sounders provide reliable properties of cirrus with an optical depth as low as 0.1, day and night (Wylie and Menzel, 1994; Ackerman et al., 1995; Stubenrauch et al., 1999; Chung et al., 2000; Kahn et al., 2004, 2007; Stubenrauch et al., 2010). $CO_2$-sensitive channels of IR vertical sounders allow the determination of cloud height and cloud emissivity, and the spectral range between 8 and 12 µm allows
20  an estimation of the $D_e$ and IWP of semi-transparent cirrus (e.g. Kahn et al., 2008; Rädel et al., 2003). This type of instrument is used to observe our planet since 1979, with improving spectral resolution: the TIROS-N Operational Vertical Sounders (TOVS) onboard the NOAA polar satellites, the Atmospheric InfraRed Sounder (AIRS) onboard Aqua (since 2002) and the InfraRed Atmospheric Sounding Interferometer (IASI) on-
25  board METOP (since 2006). The retrieval of $D_e$ relies on the fact that the spectral differences in absorption (and scattering) of radiation depends on the size of the cloud particles and also on the IWP. Whereas techniques combining visible and near IR information (e.g., Hong et al., 2007; Platnick et al., 2003; Roebeling et al., 2006) provide estimations of $D_e$ for all ice clouds (however only near the top of the cloud for optically

thick clouds), IR techniques, based essentially on the spectral absorption differences between two or more wavelengths, are restricted to semi-transparent ice clouds.

The active instruments, Cloud-Aerosol Lidar with Orthogonal Polarization (CALIOP) and Cloud Profiling Radar (CPR) of the A-Train (Stephens et al., 2002) help us to characterize the cirrus vertical structure and to study relationships with the bulk microphysical properties.

This article is structured in the following way: Sect. 2 describes essentially our AIRS retrieval method as well as the coincident data from CALIOP and CPR. After sensitivity studies in Sect. 3, we discuss the retrieval applicability in Sect. 4, Sect. 5 presents results of the statistical analysis and our findings are summarized in Sect. 6.

## 2 Data and methods

### 2.1 AIRS cloud properties

Launched in May 2002 onboard the Earth Observing System (EOS) platform Aqua, the AIRS instrument (Aumann et al., 2003; Chahine et al., 2006) provides very high spectral resolution measurements of Earth-emitted radiation in three spectral bands ($3.74 - 4.61\,\mu m$, $6.20 - 8.22\,\mu m$ and $8.80 - 15.40\,\mu m$) using 2378 channels with a spectral resolution given by $\Delta\lambda/\lambda = 0.0008$. The polar orbiting Aqua satellite provides observations at 1:30 and 13:30 local time (LT, equator crossing time). The spatial resolution of these measurements is 13.5 km at nadir. Nine AIRS measurements (3 × 3) correspond to one footprint of the Advanced Microwave Sounder Unit (AMSU), also called a golf ball.

NASA L2 atmospheric temperature and water vapor profiles (Susskind et al., 2003, 2006) are retrieved from cloud-cleared AIRS radiances (Chahine et al., 2006) within each AMSU footprint.

The Thermodynamic Initial Guess Retrieval (TIGR) dataset (Chédin et al., 1985; Chevallier et al., 1998) is composed of two sub-databases, one containing the

**Bulk microphysical properties of semi transparent cirrus from AIRS**

A. Guignard et al.

thermodynamic profiles (T,$H_2O$,$O_3$), the second with the corresponding transmissivity profiles obtained from a radiative transfer model. Special attention is given to proximity recognition between the retrieved atmospheric profiles and the ones collected in the TIGR data set. Spectral surface emissivities are determined from AIRS (Péquignot et al. (2008), calculated at the Laboratoire de Météorologie Dynamique and available at: http://ara.abct.lmd.polytechnique.fr/) in the tropics (30° N–30° S) and taken from MODIS (Seemann et al., 2008) at higher latitudes.

The LMD cloud property retrieval scheme provides cloud pressure and emissivity of a single cloud layer (of the uppermost cloud layer in the case of multi layer clouds). It is based on a weighted $\chi^2$ ($\chi^2_w$) method using eight channels around the 15 µm $CO_2$ absorption band (Stubenrauch et al., 2010). The $\chi^2_w$ method determines the pressure level for which the measured radiances at all wavelengths provide the most coherent cloud emissivity, $\epsilon_{cld}$ :

$$\epsilon_{cld}(p_k,\lambda_i) = \frac{I_m(\lambda_i) - I_{clr}(\lambda_i)}{I_{cld}(p_k,\lambda_i) - I_{clr}(\lambda_i)} \quad \text{for} \quad i = 1..8 \tag{1}$$

where $\lambda_i$ is the wavelength of AIRS channel i, $p_k$ is the pressure level $k$ out of 40 levels, $I_m$ is the measured radiance, $I_{clr}$ and $I_{cld}$ are the computed clear sky and cloudy (opaque) radiances, respectively. The $\chi^2_w$ method was developed to take into account (1) the vertical weighting of the different channels, (2) the growing uncertainty in the computation of $\epsilon_{cld}$ with increasing $p_k$ and (3) uncertainties in atmospheric profiles. When the $\chi^2_w$ method leads to a non-acceptable value of $\epsilon_{cld}$ (larger than 1.5), the scene is set to clear sky (as well as in the case of $\epsilon_{cld} < 0.05$). Cloud temperature $T_{cld}$ is determined from $p_{cld}$, using the AIRS L2 temperature profile. The cloud property retrieval is applied to all AIRS footprints. The distinction between cloudy and clear sky (or slightly cloudy so that cloud properties would not be reliable) is essentially based on the spectral coherence of cloud emissivity, using the retrieved cloud pressure. Cloud amount and cloud properties have been evaluated using two years of collocated

CALIPSO data (Stubenrauch et al., 2008, 2010): the retrieved AIRS cloud pressure of 72 % of high ($p_{cld} < 440$ hPa) and of 59 % of lowlevel ($p_{cld} > 680$ hPa) clouds lies within 75 hPa of the apparent middle (see Sect. 2.3) of the CALIPSO cloud layers.

## 2.2 AIRS bulk microphysical properties of semi-transparent cirrus

In the following we describe the methodology used to retrieve the $D_e$ and IWP of semi-transparent cirrus. The spectral behaviour of cirrus emissivity allows us to distinguish between cirrus containing mostly column-like or aggregate-like ice crystals. In a first step, the single scattering properties (SSPs) of ice crystals have been integrated into a radiative transfer model to simulate look-up tables (LUTs) of cirrus emissivities between 8 and 12 μm as function of $D_e$ and IWP. These LUTs are then used in the AIRS retrieval.

### 2.2.1 Simulation of cirrus emissivities

The calculation of the radiative impact of cirrus requires the precise knowledge of the SSPs of ice crystals. SSPs depend on the complex refractive index of the particle, on particle shape as well as on size parameter (the ratio between the characteristic particle dimension and the incident wavelength). We use extinction cross section, single scattering albedo and asymmetry parameter determined for column-like and aggregate-like ice crystals by Baran and Francis (2004). The aspect ratio of the column-like ice crystals decreases with maximum dimension and is constant for aggregate-like ice crystals.

To compute interactions between ice crystals and radiation over an entire population of randomly oriented particles, the SSPs of the individual crystals have been integrated over a bimodal size distribution, with an exponential behaviour for small ice crystals and a Γ distribution for larger ones (Mitchell et al., 1996). This kind of particle size distribution (PSD) is predicted from growth processes of water vapour deposition and aggregation (e.g. Arnott et al., 1995; McFarquar and Heymsfield, 1996) and has been

confirmed by in situ measurements (Mitchell et al., 1996; Mace et al., 1998; Field et al., 2005, 2007). The PSD used in this study was probably not affected by the shattering problem (Mitchell et al., 2011).

This population is characterized by its crystal habit and by its ice-crystal mean $D_e$ which is considered as an effective photon path through the PSD (before internal reflection takes place). It can be calculated, according to Mc Farquhar and Heymsfield (1997) and Mitchell et al. (2002), as the ratio of total volume to total projected area of the entire crystal population as in Eq. (2):

$$D_e = \frac{3}{2} \frac{\int_0^\infty V\,n(r)\,\mathrm{d}r}{\int_0^\infty P\,n(r)\,\mathrm{d}r} \tag{2}$$

where $V$ and $P$ are the volume and projected area of an ice crystal in a size distribution $n(r)$ with respect to radius.

These SSPs are then implemented, as a function of $D_e$ and wavelength, into the line-by-line Automatized Atmospheric Absorption Atlas (4A) radiative transfer model (Scott and Chédin, 1981) coupled (Pierangelo et al;, 2005) with a multiple scattering model based on discrete ordinate radiative transfer (DISORT, Stamnes et al., 1988). Cloud, atmospheric and surface properties for simulation of cirrus emissivities are the same as in Rädel et al. (2003): cloud top height is 10 km (corresponding to cloud top temperature of 237 K), cloud vertical extent is 1 km, surface temperature is 300 K, lapse rate is 6.5 K km$^{-1}$ and surface emissivity is set to 1. Section 3 describes sensitivity studies linked to changes in these parameters. To determine the cirrus spectral emissivity, we also need to simulate radiances for clear sky and for an opaque cloud situated at the same height as the cirrus. Spectral cirrus emissivities are then calculated in the same manner as in Eq. (1), only with $I_m$ also depending on $D_e$ and IWP.

For the retrieval application we construct LUTs composed of spectral cirrus emissivities between 8 and 12 μm depending on the $D_e$ and IWP, with the $D_e$ varying from 7 to 85 μm and the IWP varying from 1 to 120 g m$^{-2}$, separately for two different ice crystal

habits (column-like and aggregate-like) and for eight different viewing angles between 0 and 30° (see Sect. 4). We note that by using cirrus emissivities instead of brightness temperatures, the surrounding atmosphere is taken into account (Rädel et al., 2003); therefore, one does not need to produce LUTs for different atmospheres.

Figure 1 presents the simulated range of $D_e$ and IWP for a given emissivity at 12 μm of a cloud composed of aggregate-like ice crystals. Whereas the range of $D_e$ is the same, the range of IWP increases with increasing cirrus emissivity. For a given emissivity and larger $D_e$ the total extinction is large and therefore the resulting IWP is also large.

Figure 2 presents the normalized spectral emissivities differences, compared to the emissivity at 12 μm, as a function of wavelength, separately for column-like and aggregate-like ice crystals. We present simulations for a small IWP of 10 g m$^{-2}$ and for a larger IWP at 20 g m$^{-2}$, each distinguishing three values of $D_e$ (10, 30 and 50 μm). Wavelengths between 8 and 10 μm are the most sensitive to $D_e$ variation. We note that the sensitivity to $D_e$ will decrease with increasing IWP. It appears that the cirrus emissivity between 8 and 10 μm is also sensitive to crystal habit with larger emissivity differences for aggregate-like ice crystals than for columns-like ice crystals.

To better illustrate the cirrus emissivity range for which a retrieval of $D_e$ is possible, Fig. 3 presents ice cloud emissivity differences between 12 and 9 μm ($\Delta\epsilon_{12-9}$) as a function of ice cloud emissivity at 12 μm for various mean effective ice crystal diameters. For a given cirrus emissivity at 12 μm ($\epsilon_{12}$), which corresponds to a certain IWP, $\Delta\epsilon_{12-9}$ increases with decreasing $D_e$. The difference is maximum for a semi-transparent cirrus of $\epsilon_{12} \simeq 0.7$ and becomes zero if the emissivity reaches 0 or 1. This figure is similar to the one for TOVS, using a cirrus emissivity difference between 11.1 and 8.3 μm (Rädel et al., 2003).

However, we have more spectral information available with AIRS: we have selected two channels in the range around 9 μm, two channels around the slope between 10 and 11 μm, and the average of two channels around 12 μm (indicated in black in Fig. 2) for the retrieval. By using more channels among the ones which worked properly during

the whole period, we obtained similar results and it has been shown by L'Ecuyer et al., 2006 and Kahn et al., 2008) that cloud property retrieval does not improve anymore by adding additional spectral information when the most sensitive channels are already being used.

### 2.2.2 Retrieval

Once the physical cloud properties ($p_{cld}$ and $\epsilon_{cld}$) are determined (see Sect. 2.1), six spectral emissivities at $8.87, 9.12, 10.41, 10.70, 12.02$ and $12.33\,\mu m$ are determined for high clouds ($p_{cld} < 440\,hPa$). For the assumed ice crystal habits (column-like or aggregate-like) the retrieved $D_e$-IWP couple is given by Eq. (3). The cirrus emissivities ($\epsilon^m$) are compared with the LUT's ($\epsilon^s$) and proximity recognition, weighted by the root mean square of the spectral variability of the emissivities, is applied.

$$\Delta_{\theta_v}(D_e, \text{IWP}) = \frac{\sum_{i=1}^{6}(\epsilon^m_{\lambda_i,\theta_v} - \epsilon^s_{\lambda_i,\theta_v}(D_e,\text{IWP}))^2 \cdot \sigma(\epsilon^s_{\lambda_i,\theta_v})}{\sum_{j=1}^{6}\sigma(\epsilon^s_{\lambda_j,\theta_v})} \tag{3}$$

where $\lambda_i$ represents the $i$-th channel selected, $\theta_v$ is the viewing angle and $\sigma(\epsilon^s_{\lambda_j,\theta_v})$ is the root mean square of the simulated emissivity for a particular channel and a particular viewing angle.

### 2.3 Cloud vertical structure from Radar-Lidar GEOPROF data

The lidar CALIOP (Winker et al., 2007, 2009) of the CALIPSO mission, provides backscatter profiles at $532\,nm$ and at $1064\,nm$ with a vertical and horizontal resolution of about $30\,m$ and $90\,m$, respectively. Horizontal sampling is $333\,m$ along the track and the distance between two orbits is about $1000\,km$. CALIPSO provides information on the geometrical height of cloud top and apparent cloud base. The latter is higher than the real cloud base in the case of optically thick clouds where the lidar signal

penetrates the cloud only up to an optical depth of about 5 (Winker et al., 2003). The radar CPR of the Cloudsat mission (Stephens et al., 2002), is a 94 GHz nadir-viewing radar which measures the profile of the power backscattered by clouds at a vertical resolution of about 250 m and with an horizontal resolution of about 2.5 km × 1.4 km.

5  It is able to probe optically thick cloud layers and therefore provides the correct cloud base. Combining these two instruments has the potential of providing a complete description of the vertical structure of clouds. However, one has to remember that the laser-like view of these platforms means that they observe only a small fraction of all cloudy scenes. In this study we use the L2 Radar-Lidar GEOPROF data (Version 3,

10  Mace et al., 2009) that merge the geometrical profiling of CALIOP and CPR. The AIRS data have been collocated with the L2 Radar Lidar GEOPROF data (Stubenrauch et al., 2010). In addition, we determine horizontal scene homogeneity by using cloud type information (according to $p_{cld}$ and $\epsilon_{cld}$) of the 3 × 3 AIRS footprints per AMSU golf ball. For the analysis of semi transparent high ice clouds, we only keep situations

15  with overcast AMSU golf balls (all AIRS footprints are cloudy) and for which the AIRS cloud radiative altitude lies between the top and the base altitude determined by the Radar-Lidar sample.

## 3   Sensitivity studies

When creating Look Up Tables (Sect. 2.2.1), we had to make several assumptions on
20  the physical parameters of the cloud as well as on the ice crystals. In this section, we study the uncertainties on the retrieved $D_e$ associated with these assumptions. We resume the standard conditions for the simulation of ice cloud spectral emissivities:

- vertical extent $Z_{cld} = 1$ km

- cloud height $h_{cld} = 10$ km, correspondingto $T_{cld} = 237$ K in the tropics

25  - randomly-oriented aggregate-like ice crystals integrated over a bimodal Γ size distribution

– atmospheric lapse rate equal to $6.5 \, \text{K km}^{-1}$

– surface temperature $T_s = 300 \, \text{K}$

– surface emissivity $\epsilon_s = 1$

## 3.1 Sensitivity to atmospheric properties

We have independently made the following changes: increasing cloud vertical extent by 1 km, cloud height by 4 km (decreasing $T_{cld}$ by 27 K), increasing atmospheric lapse rate to $11.5 \, \text{K km}^{-1}$ and decreasing surface temperature by 15 K. The resulting differences in the initially retrieved $D_e$ called $D_e^{std}$ compared to the retrieval with the new parameter called $D_e'$ are presented in the upper part of Table 1. The differences are normalized to $D_e^{std}$, and are shown separately for optically thin clouds ($\epsilon_{12\,\mu m} \simeq 0.3$) and relatively thick clouds ($\epsilon_{12\,\mu m} \approx 0.75$) and also for small and large $D_e$ ($D_e \simeq 19 \, \mu m$ and $D_e \simeq 60 \, \mu m$, respectively). In general, all changes are small and lie around 1 % to 2 %. Only the lapse rate increase in the case of optically thin clouds consisting of small particles leads to a decrease of 6 %. In addition, we increased the vertical extent up to 5 km which is a relevant extent according to Fig. 4. For clouds with vertical extents between 4 and 5 km, the uncertainty remains small for optically thick cirrus ($D_e'$ 1 % smaller than $D_e^{std}$). For optically thin cirrus and small particles, $D_e'$ can be up to 10 % smaller than $D_e^{std}$ but these cases are very rare.

To evaluate the effect of horizontal heterogeneity, we have compared results obtained for golf balls containing only cirrus to those obtained for golf balls containing also other cloud types (but that are fully cloud covered: overcast golf balls). The hypothesis is that heterogeneous scenes have a higher probability for an AIRS footprint to be partially covered by an ice cloud and by a low cloud. When including heterogeneous overcast scenes (which add 12 % to the statistics of golf balls that are entirely covered by cirrus), the retrieved $D_e$ is only 3 % smaller. However, including partially cloud-covered footprints (not surrounded by other cloudy footprints), $D_e$ can be up to 10 %

smaller than in the case of a fully covered AIRS footprint. The population of partially cloud- covered golf balls is, on a global scale, 10 times smaller than the population of overcast golfballs. A partially covered AIRS footprint leads to an overestimation of $D_e$ that is smaller than the one mentioned in (Rädel et al., 2003) for the TOVS retrieval.
5  This is partly due to the better spatial resolution of the AIRS retrieval (13 km instead of 100 km for TOVS). To minimize the uncertainty due to horizontal heterogeneity but keeping an important statistics we decide to keep only overcast golf balls.

## 3.2 Sensitivity to ice crystal properties

The first sensitivity study concerns other ice crystal shapes and approaches to de-
10  termine the single scattering properties. Whereas SSPs by Baran (2004) have been determined using the T-Matrix approximation, the SSP determination by Mitchell (1996, 2002) is based on the Anomalous Diffraction Approximation. Comparisons by Mitchell et al. (2006) have shown a good agreement between both methods. Therefore, only the difference in shape remains: aggregated columns (Baran) compared to aggregated
15  plates (Mitchell). For each case, cirrus emissivities were calculated using the same crystal size distribution. The lower part of Table 1 presents normalized differences between $D_e^{std}$ and newly retrieved $D_e'$, separately for optically thin and thick cirrus and separately for small $D_e$ and large $D_e$. Differences are small, lying around −1 % to −2 %, assuming aggregated plates instead of aggregated columns.
20    The retrieval also provides an estimation of the most probable ice crystal shape. For each event it retains the two best fits for each crystal habit and then compares the overall best fit to the second best fit. For most of the cases, the first and second best fits of $D_e$ stem from the same ice crystal habit (96 % and 87 % for small and large particles respectively), and so the uncertainty on the retrieved $D_e$ is quite small and lies within
25  4 % (this uncertainty is smaller for large particles in an optically thick cloud and slightly larger for column-like than for aggregate-like ice crystals). When the two best fits do not present the same habit (4 % and 13 % for small and large particles respectively), $D_e$ uncertainties remain small within a few percent, (slightly larger for optically thin clouds).

**Bulk microphysical properties of semi transparent cirrus from AIRS**

A. Guignard et al.

Therefore, even when a particular shape can not be distinguished, the uncertainty on $D_e$ remains very small. In this case, we choose to average the two effective diameters and the shape is set to uncertain.

## 4  Retrieval applicability

We apply the retrieval of bulk microphysical properties to all AIRS footprints supposed to be covered by ice clouds. Therefore, we select footprints of overcast golf balls, containing high clouds ($p_{cld} < 440$ hPa) with $T_{cld} < 260$ K (as the distinction for ice clouds by the International Satellite Cloud Climatology Project (ISCCP, Rossow and Schiffer, 1999). For each of these two cloud properties, we compare the best $\chi^2_w$ solution with the second best one (Sect. 2.1) and keep only those clouds with stable solutions. In addition, we reject AIRS footprints with a viewing zenith angle greater than 30°, because the IWP corresponds to a trajectory considerably longer than the cloud vertical extent. In a first step, no particular attention is accorded to the cloud effective emissivity except to be between 0 and 1. These cuts leave us with the basic population of high clouds which will be referenced as HC hereafter. In this section we investigate the relationships between the bulk microphysical properties and the physical cloud properties.

### 4.1  Relationship with cloud effective emissivity

As already seen in Fig. 3, the retrieval is not sensitive anymore to $D_e$ for clouds with low and high emissivity. In Fig. 5, we present the retrieved bulk microphysical properties as a function of the AIRS cloud emissivity determined by the $\chi^2_w$-method separately for different latitude bands and different seasons. To determine the range of cloud emissivity in which the bulk microphysical properties are well retrieved, we study their behaviour. We observe that the fraction of uncertain shape (Sect. 3.2) is larger for low cloud emissvities, with a large spread between the different regions for $\epsilon_{cld} < 0.20$, and drops to nearly 0 when $\epsilon_{cld} > 0.85$ as well as the fraction of aggregate-like ice crys-

tals. $D_e$ increases slightly with $\epsilon_{cld}$ but we observe a change in the slope of increase for $\epsilon_{cld} \simeq 0.2$ and $\epsilon_{cld} \simeq 0.85$. IWP strongly increases with $\epsilon_{cld}$ and then stays constant and even drops for $\epsilon_{cld} > 0.85$. All these behaviours lead us to the conclusion that the retrieval of bulk microphysical properties can be conducted for AIRS for $\epsilon_{cld}$ between 0.2 and 0.85, corresponding to semi-transparent cirrus. It is interesting to note that within this range, IWP behaves the same for all latitude bands and seasons, the behaviour of $D_e$ is similar, except with smaller values and a slightly stronger increase in the Southern Hemisphere (SH) midlatitude summer. The fraction of aggregate-like ice crystals also increases with $\epsilon_{cld}$, reaching 0.6 for $\epsilon_{cld} > 0.55$. There is a spread of about 0.1 between the different latitude bands and seasons, with less complex shapes in Northern Hemisphere (NH) mid-latitudes during winter. These thresholds are consistent with previous studies (Rädel et al., 2003). For optically thin clouds the atmosphere plays a more important role, and it has been shown that choosing a wrong atmospheric profile can lead to a bias in $D_e$. In Rädel et al. (2003), the lower emissivity threshold for TOVS was fixed at $\epsilon_{cld} = 0.3$, but the improvement of the spectral and spatial resolution of the AIRS instrument allows us to reduce this value to $\epsilon_{cld} = 0.2$. Bulk microphysical properties of these semi-transparent cirrus correspond to an average over the whole cloud vertical extent (Rädel et al., 2003), whereas for optically thick clouds, the instrument only sounds the upper part of the cloud (Sect. 5.2.2).

## 4.2 Distinction between ice clouds and mixed phase clouds

We study the microphysical properties as a function of cloud temperature. In Fig. 6, when considering the different latitude bands and seasons, we distinguish two regimes:

- $T_{cld} < 230\,\text{K}$ : $D_e$ and IWP increase with increasing $T_{cld}$ and the fraction of aggregate-like ice crystals ($\simeq 0.6$) remains approximately constant.

- $T_{cld} > 230\,\text{K}$ : $D_e$ and IWP decrease with increasing $T_{cld}$ and the fraction of column-like ice crystals strongly increases with increasing $T_{cld}$

The change in behaviours of $D_e$ and IWP at 230 K as well as the increase of the rate of columns-like ice crystals (the latter have SSPs closer to spheres than aggregate-like ice crystals) demonstrate that pure ice clouds only occur when $T_{cld} < 230$ K. This is in agreement with previous studies (Yang et al., 2002; Hu et al., 2009; Riedi et al., 2010; Martins et al., 2011). It also seems from Fig. 6 that the temperature does not much affect the crystal shape in pure ice clouds, which is consistent with the fact that the roundness of particles is a weak function of temperature (Korolev and Isaac., 2003).

## 4.3 Occurrence of semi-transparent high ice clouds

From the findings in Sects. 4.1 and 4.2 we conclude to consider in the following only Semi-Transparent High Clouds of pure ice, referenced as ST-HIC and defined as below:

| | |
|---|---|
| high clouds: | $p_{cld} \leq 440$ hPa |
| pure ice clouds: | $T_{cld} \leq 230$ K |
| semi-transparent clouds: | $0.2 \leq \epsilon_{cld} \leq 0.85$ |
| (corresponding to visible optical depth: | $0.4 \leq \tau_{vis} \leq 3.8$) |

Globally the cut on cloud emissivity retains about 70 % of high clouds, slightly more over land than over ocean (see Table 2). Figure 7 presents distributions of $T_{cld}$, in NH mid-latitudes, the tropics and SH mid-latitudes, separately in boreal winter and in boreal summer. We observe a strong summer-winter difference in the mid-latitudes and much broader distributions in the tropics. While in the mid-latitudes more than 60 % of semi-transparent cirrus present a temperature lower than 230 K in winter and only less than 20 % in summer, this rate is almost constant in the tropics (55 %). The seasonal difference is stronger over ocean than over land (Table 2). Cuts on cloud emissivity do not present any particular seasonal cycle. However $\epsilon_{cld}$ (Fig. 9), is in general larger in the mid-latitudes (frontal systems) than in the tropics (anvils), and in the mid-latitudes values are in general lower in summer than in winter. On the right column of Fig. 4, the $\epsilon_{cld}$ distributions of ST-HIC, in NH mid-latitudes, tropics and SH mid-latitudes are

A. Guignard et al.

Title Page

| Abstract | Introduction |
| Conclusions | References |
| Tables | Figures |

◀◀  ▶▶

◀  ▶

Back  Close

Full Screen / Esc

Printer-friendly Version

Interactive Discussion

presented, separately in boreal winter and in boreal summer. Distributions are not Gaussian and present two peaks at low and large values. In the NH mid-latitudes, the seasonal cycle of ST-HIC effective emissivity has been reinforced by cuts on temperature and in summer the emissivity presents almost the same distribution as in the tropics, in contrary to SH mid-latitudes where the seasonal cycle is weaker. This may be linked to the atmospheric general circulation. Figure 8 presents geographical maps of the relative high cloud amount (scaled to total cloud amount) and relative semi-transparent high ice cloud amount over the period 2003–2009. ST-HIC amount is significantly smaller than HC amount but follows the same geographical pattern. Associated statistics are resumed in Table 3. The Inter Tropical Convergence Zone (ITCZ) presents the highest relative HC amount and relative ST-HIC amount (about 15 % of all clouds or 25 % of high clouds) with almost no difference between ocean and land. Relative HC amount presents a significant seasonal difference in the SH mid-latitudes whereas it is nearly constant in the NH mid-latitudes. On the contrary, the seasonal difference of the relative ST-HIC amount is pronounced in both hemispheres. Mainly because of temperature distributions, ST-HIC occur mostly during winter where they represent practically 30 % of high clouds. We also note that the relative ST-HIC amount is significantly higher over land than over ocean.

## 5  Analysis of $D_e$, IWP and ice crystal habit

### 5.1  Geographical and seasonal variations

Figure 9 shows geographical maps of ST-HIC effective emissivity and IWP, separately for boreal winter and for boreal summer, averaged over the period 2003–2009. As already observed in Fig. 5, these two parameters are highly correlated. Cold and moist air masses generate cirrus with large IWP and infrared emissivity. The largest values are encountered in the mid-latitudes in winter and can be associated to winter storm-tracks. The ITCZ is apparent, though less than in the geographical maps of ST-

HIC amount, by middle range values of both IR emissivity and IWP. Figure 10 shows geographical maps of $D_e$ and the dominating ice crystal shape, separately for boreal winter and for boreal summer. As IR emissivity and IWP, $D_e$ is larger in winter than in summer in the mid-latitudes.

On a global scale, the most representative form of ice crystals seems to be aggregate-like. That is consistent with in situ measurements that suggest that irregular is the dominant habit of ice particle grown in natural clouds (Francis and Foot, 1999; Korolev and Isaac., 2003; Gayet et al., 2011). Nevertheless, in the SH mid-latitudes during summer, in some oceanic regions of the NH, mid-latitudes and generally over land ST-HIC seems to be mainly composed of column-like ice crystals. On average, the fraction of ice clouds containing aggregate-like ice crystal shapes is about 44 %, 54 % and 55–60 % in the NH mid-latitudes tropics and SH mid-latitudes, respectively. Figure 11 presents for different latitude bands and seasons correlations of the fraction of aggregate-like ice crystals with IWP(top) as well as with $D_e$ (below). We note that the fraction aggregate-like ice crystals increases with IWP, thus explaining the higher frequency of this shape in the mid-latitudes during winter. For a fixed IWP, the fraction of aggregate-like ice crystals decreases with increasing $D_e$.

This is consistent with in situ measurements that show that the shape of ice crystals becomes less spherical as its size increases (Mitchell., 2009). Figure 12 presents normalized frequency distributions of the microphysical properties ($D_e$, IWP and shape) for three latitude bands (NH mid-latitudes, tropics and SH mid-latitudes), separately for boreal summer and for boreal winter. Table 4 presents averages, also separately over ocean and over land. For the bulk microphysical properties ($D_e$ and IWP) we present the medians of the distributions. These are very similar to the averages, but about 10 % smaller. In general, IWP distributions are very asymmetric, with a peak around $10 \, \mathrm{g \, m^{-2}}$ and a long tail towards large values. Whereas in the tropics there is no seasonal difference, with a median value of about $20 \; \mathrm{g \, m^{-2}}$, there are more ST-HICs with small IWP in summer than in winter in the mid-latitudes, leading to differences in the median of about $10 \, \mathrm{g \, m^{-2}}$. In the SH the winter peak is even shifted towards a

larger value.

## 5.2 Relationship with cloud vertical structure

### 5.2.1 Single and multi layer clouds

The Radar-Lidar GEOPROF data that have been collocated with AIRS data, allow us to characterize the vertical structure of the ST-HIC. Figure 13 presents geographical maps of the fraction of single layer clouds and of the vertical extent of the ST-HIC population, separately for boreal winter and for boreal summer. The relative amount of single layer ST-HIC is presented in the column named %SL of Table 4, separately for the three latitude bands and for boreal winter and boreal summer. In general, we observe less single layer ST-HICs in the tropics and in the case of winter storm tracks in the mid-latitudes and more single layer ST-HICs over land, especially in the mid-latitudes. Single layer ST-HICs also largely dominate over the Sahara. The vertical extent of the uppermost ST-HICs in multi layer systems is in general smaller than the one in single layer ST-HICs, in agreement with other general cloud observations (e.g. Wang et al., 2000). We observe the smallest averages in regions where no convection occurs. ST-HICs are on average vertically more extended in the mid-latitudes (especially in the SH and in winter in the NH) than in the tropics, except over very small areas of intense convection over land. Comparing bulk microphysical properties, single layer and multi layer ST-HICs present similar distributions (not shown) but contain larger values for a single layer. It also seems that the fraction of aggregated columns is slightly larger for single layer than for multi layer ST-HICs.

### 5.2.2 Dependance with cirrus geometrical depth

Figure 14 presents the dependency of bulk microphysical properties on the cloud vertical extent for different latitude bands and seasons, separately over ocean and over land. In general, the ST-HIC emissivity increases with vertical extent. No seasonal

A. Guignard et al.

Title Page

| Abstract | Introduction |
| Conclusions | References |
| Tables | Figures |

Back | Close

Full Screen / Esc

Printer-friendly Version

Interactive Discussion

differences are observed in the tropics and SH mid-latitudes, whereas for NH mid-latitudes the behaviour corresponds more to the one in the tropics during summer and to the one in the SH mid-latitudes during winter. Cirrus over ocean and over land demonstrate a similar behaviour. It is interesting to note that for the same vertical extent, the emissivity of clouds is largest in the SH mid-latitudes and smallest in the tropics. This is probably linked to the different types of cirrus, those from anvils in the tropics and those from waves and storms in the mid-latitudes. However, their IWP is very similar and constant for cloud vertical extent up to 4 km, and then it increases for ST-HICs in the mid-latitudes and much less for ST-HICs in the tropics. In general, $D_e$ shows a similar behaviour as a function of vertical extent, with even smaller changes with vertical extent. However, at the same vertical extent, ST-HICs have slightly larger $D_e$ in the tropics and NH mid-latitude summer than in the SH mid-latitudes and in NH mid-latitude winter.In fact, it appears that the bulk microphysical properties depend essentially on the optical thickness and are almost independent of the vertical extent of the cloud. One exception is the behaviour of ST-HICs over NH mid-latitudes land in winter, with smaller column-like ice crystals for ST-HICs with less vertical extent and larger crystals in geometrically thicker ST-HICs.

## 5.3 Comparison with TOVS

Bulk microphysical properties of semi-transparent cirrus have already been retrieved with the TIROS-N Operational Vertical Sounder (TOVS) (Rädel et al., 2003; Stubenrauch et al., 2004). The methodology is similar, with the following main differences compared to our AIRS retrieval: single scattering properties have been determined by assuming ice crystals as aggregated plates (Mitchell et al., 1996), only two channels (at 8.3 and 11.9 μm) were available and therefore first $D_e$ (using LUTs depending on $\epsilon_{cld}$ at 8.3 and 11.9 μm) and in a second step IWP (using LUTs depending on $D_e$ and $\epsilon_{11}$) were retrieved, for semi-transparent cirrus ($0.3 < \epsilon_{cld} < 0.85$ ) over the period 1989–1990. Another important difference is the spatial resolution of the retrievals: 100 km for TOVS compared to 13.5 km for AIRS.

In Fig. 15, we compare the global annual distributions of $D_e$ and IWP from TOVS and AIRS separately for several cirrus emissivity intervals. We also include results from a retrieval using the two AIRS channels that are the closest to the TOVS ones, for aggregate-like ice crystals only. All distributions consider clouds with $T_{cld} < 230$ K.

In general, the overall distributions (lowest panel) agree quite well, with a slightly wider IWP distribution from AIRS. Considering the different cirrus emissivity intervals, we observe that both instruments provide very similar results on $D_e$ and IWP for $\epsilon_{cld}$ between 0.5 and 0.7, which corresponds to the range of maximum sensitivity (Fig. 3 and Fig. 1 of Rädel et al., 2003). Differences appear when considering smaller and larger emissivities, for which the TOVS spectral cirrus emissivity differences are smaller and larger than the ones of AIRS, respectively (not shown). This leads to larger and smaller $D_e$ obtained by TOVS for optically thin and optically thicker clouds, respectively, compared to those obtained by AIRS. Assuming that the better spectral and spatial resolution of AIRS has led to improvements in the retrieval, a slight overestimation of $D_e$ by TOVS for clouds with small emissivity could be explained by partial cloud cover or spatial heterogeneity (Table 1 of Rädel et al., 2003). The better spectral resolution and the additional channels at wavelengths greater than 8.3 µm of AIRS lead to a slightly deeper sounding (see Fig. 8 of Rädel et al., 2003), which in the case of optically thicker clouds (see Fig. 15) leads therefore to larger $D_e$ (if one assumes that $D_e$ increases from cloud top to cloud base are due to aggregation). From Fig. 15, we also observe that in general, IWP increases with $\epsilon_{cld}$. We observe however a stronger increase by using AIRS than by using TOVS. This is because $D_e$ obtained from AIRS also increases with $\epsilon_{cld}$. Moreover, the IWP distributions from AIRS become wider, whereas those from TOVS stay quite narrow. This is probably due to the fact that the TOVS two channel method first determines $D_e$ and then IWP from $D_e$ and $\epsilon_{cld}$, whereas the AIRS multi-channel method extracts $D_e$ and IWP simultaneously.

## 5.4   $D_e$ parameterization

As mentioned in the introduction, cirrus bulk microphysical properties depend on many environmental factors. However, for modelling cirrus radiative effects in GCMs), $D_e$ has to be predicted from other variables. Simple relationships between temperature, ice water content and $D_e$ have been suggested (Kristjansson et al., 2000; Ou and Liou, 1995; Donovan and van Lammeren, 2002). Our global data set allows us to examine such relationships and to verify if a global parameterization may be found suitable for GCMs. Figure 16 presents the correlation between $D_e$ and IWP, separately for the three latitude bands, each for three cloud temperature intervals. A positive correlation exists between these two variables, already revealed by different field campaigns (Mitchell et al., 1996; Korolev et al., 2001). We note a rapid growth of $D_e$ for IWP smaller than $20\,\mathrm{g\,m^{-2}}$. For larger IWP values, the increase becomes weaker but remains strong compared to studies above where the relationship rapidly tends to become flatter. The same is true for the relationship between $D_e$ and IWP obtained from collocated Scanner of Radiation Balance (ScaRaB) and TOVS data in Stubenrauch et al. (2007) (black dashed line). The difference in behaviour may be explained by the deeper sounding (see Sect. 5.2.2) and also by the fact that we only consider pure ice clouds with $T_{\mathrm{cld}} < 230\,\mathrm{K}$, whereas retrieved microphysical properties for clouds with temperatures lower than 260 K may contain smaller liquid water droplets. The parameterization of $D_e$ as a function of IWP that fits best the data observed at the global scale (full black line) is described by the expression:

$$D_e(\mathrm{IWP}) = \sum_{i=0}^{4} \alpha_i \cdot ln(\mathrm{IWP})^i \tag{4}$$

with $\alpha_0 = 9.945$, $\alpha_1 = -11.245$, $\alpha_2 = 27.426$, $\alpha_3 = -9.192$ and $\alpha_4 = 0.974$.

We studied the robustness of the parameterization by randomly separating the data set into two halves and refitting the data again. The coefficients were stable within

0.005. For a fixed IWP, when considering the different latitude bands and cloud temperature intervals, the overall spread of $D_e$ is about 10 %. This indicates that $D_e$ depends strongly on IWP (which itself is also related to cloud temperature as shown in Fig. 6), and only slightly on cloud temperature in addition. Considering the different latitude bands, one even observes a different behaviour in tropics and mid-latitudes: for cirrus with the same IWP, $D_e$ increases with $T_{cld}$ in the tropics whereas it decreases in the mid-latitudes.

Previous studies (Ivanova et al., 2001; Boudala et al., 2002; Edwards et al., 2007) used the temperature to parameterize $D_e$. We found that these parameterizations, generally established for clouds warmer than 230 K, underestimate the mean effective ice crystal diameter by about 10 to 20 µm compared to our data (not shown). $D_e$ varies only about 10 to 20 µm within the temperature range between 200 and 230 K and the spread of $D_e$ for a fixed temperature is also larger than the one for a fixed IWP, another sign that the dependence on IWP is more important (Baran et al., 2009). Compared to a parameterization developed for in situ measurements at a specific latitude band as for example by Boudala et al. (2002), it is difficult to determine a global multivariate parameterization for $D_e$ dependent on both IWP and temperature, because IWP and temperature present a weak dependence which varies with regions and seasons (Fig. 6).

Since field experiments present $D_e$ parameterized as a function of ice water content (IWC) (references above) and IR sounders only provide the integrated IWC (which is the IWP), we make use of the synergy with radar-lidar GEOPROF data to provide an estimation of IWC. Therefore, we determine IWC as the ratio between IWP and the vertical extent of the cloud layer, by assuming a vertically constant IWC. This assumption is only realistic for cirrus with a relatively small vertical extent (Seo and Liu, 2006).

Figure 16 presents the correlation between $D_e$ and IWC, separately for the three latitude bands in boreal winter and summer and for clouds with a vertical extent lower than 1 km and lower than 2 km. The statistics of two years are not sufficient to separate into different temperature intervals. A positive correlation exists between these

two variables, already revealed by different field campaigns ( Korolev et al., 2001; Mc Farquhar et al., 2003; Heymsfield et al., 2003; Garrett et al., 2004). We note a rapid growth of $D_e$ for IWC smaller than $0.025\,\mathrm{g\,m^{-3}}$. For larger IWC values, the increase becomes weaker but flattens less compared to the studies above. One reason is that we only consider clouds with a relatively small vertical extent. We deduce further from Fig. 17 that for cirrus with low IWC, $D_e$ increases more strongly for geometrically thicker clouds than for geometrically thinner clouds. The parametrization of $D_e$ as a function of IWC that fits best the data obsreved at the global scale (full black lines) is described by the equation:

$$D_e(\mathrm{IWC}) = \sum_{i=0}^{2} \alpha_i \cdot \ln(\mathrm{IWC})^i \tag{5}$$

with the following parameters for different vertical extents:

$\Delta Z < 1\,\mathrm{km}$:  $\qquad \alpha_0 = 92.608\ \alpha_1 = 16.544,\ \alpha_2 = -5.126$

$\Delta Z < 2\,\mathrm{km}$:  $\qquad \alpha_0 = 83.582,\ \alpha_1 = 3.981,\ \alpha_2 = -6.319$

Some GCMs use a parameterization of $D_e$ as a function of IWC at each pressure layer in which there is enough humidity to form clouds. The vertical cloud extent is determined by the number of adjacent cloud layers. However, it should be noted that this kind of parameterization depends for geometrically thicker clouds on the position relative to the cloud top. Therefore, it could be interesting for radiative flux computations to use the parameterization between $D_e$ and IWP.

## 6 Conclusions

We have conducted a retrieval and a climatological analysis of the microphysical properties of semi-transparent ice clouds using AIRS observations.

The retrieval is based on a look-up table approach, for which cirrus emissivities in the spectral range between 8 and 12 μm have been simulated as a function of $D_e$ and IWP. Therefore single scattering properties of randomly oriented column-like or aggregate-like ice crystals, distributed according to a bimodal-Γ size distribution, have been implemented into the radiative transfer model 4A-OP. Sensitivity studies lead in general to the same conclusions as an earlier study using TOVS data Rädel et al. (2003), with even lower uncertainties linked to assumptions of atmospheric parameters and horizontal homogeneity (in general less than 5 %), essentially because of spatial and spectral resolution improvements of the AIRS instrument. Uncertainties due to ice crystal habit are also small (less than 5 %). Nevertheless, the use of six channels between 8.5 and 12.5 μm allows a distinction between column-like and aggregate-like ice crystals.

Our retrieval is applicable to clouds with an effective emissivity from 0.2 to 0.85, compared to a range from 0.3 to 0.85 for a retrieval using TOVS data. By studying the relationship between retrieved bulk microphysical properties and cloud temperature, we revealed that pure ice clouds exist only at temperatures below 230 K, which is consistent with theoretical and in-situ studies. Therefore, our retrieval of bulk microphysical properties only considers semi-transparent high ice clouds (ST-HIC) that represent almost 15 % of all clouds and up to 30 % of high clouds during midlatitude winter.

For these clouds, $D_e$ and IWP increase with cloud temperature. The averages of effective emissivity, IWP and $D_e$, as well as the vertical extent and the amount of multiple cloud layers, present a strong seasonal cycle in the mid-latitudes, the larger values being associated with winter storm-tracks, in contrary to the tropics that present constant middle range values. Whereas the NH mid-latitudes show more seasonal difference in effective cloud emissivity and vertical extent, the SH mid-latitudes show a larger seasonal difference in $D_e$, IWP and fraction of aggregate-like ice crystal habit. In general ST-HIC in the SH mid-latitudes during summer have a larger effective emissivity and vertical extent but smaller $D_e$ than those in the NH mid-latitudes during summer. These

A. Guignard et al.

differences have to be studied further in relation with dynamical parameters. Concerning the estimation of ice crystal shape, on a global scale and consistent with in-situ measurements, the most representative shape appears to be aggregate-like. On the other hand, the column-like ice crystal shape dominates over land.

The use of the Radar-Lidar GEOPROF data demonstrates that the retrieved bulk microphysical properties depend essentially on cloud optical thickness (or emissivity) and are almost independent of their vertical extent.

The comparison with TOVS has shown a good agreement on the overall distributions. Nevertheless, it appears that the better spatial resolution and deeper sounding of AIRS due to the use of additional channels leads to an increased sensitivity on microphysical properties for optically thin and thicker cirrus. Whereas IWP increases with effective cirrus emissivity in both datasets, the IWP distributions obtained from AIRS are broader, because $D_e$ also increases, in contrary to those retrieved from TOVS.

The large extent of this global study, the reliability of the method and consistency with in-situ measurements allowed us to study relations between cloud bulk microphysical properties of relevance to GCM parametrizations. Whereas the relationship between $D_e$ and cloud temperature is only weak and depends on many other factors, we have shown that a parameterization of $D_e$ as a function of IWP is more robust than one as a function of temperature. The spread of $D_e$ due to other factors is only about 10%. By using the synergy with Radar-Lidar GEOPROF data and assuming a vertically constant IWC, we have also investigated a parameterization of $D_e$ as a function of IWC for cirrus with relatively small vertical extent.However, it should be noted that this kind of parameterization depends for geometrically thicker clouds on the position relative to the cloud top.

Therefore, it could be interesting for radiative flux computations to use a parameterization between $D_e$ and IWP, before $D_e$ and IWC profiles have been investigated on a global scale, for example using CALIPSO and CloudSat.

# References

Ackerman, S. A., Smith, W. L., Collard, A. D., Ma, X. L., Revercomb, H. E., and Knuteson, R. O.: Cirrus cloud properties derived from high-spectral resolution infrared spectrometry during FIRE II, Part II: Aircraft HIS results, J. Atmos. Sci., 52, 4246–4263, 1995. 24673

Arnott, W. P., Dong, Y. Y. and Hallett, J.: Extinction efficiency in the infrared A218 mmB of laboratory ice clouds: observations of scattering minima in the Christiansen bands of ice, J. Opt. Soc. Am., 34, 541–551, 1995.

Aumann, H. H., Chahine, M. T., Gautier, C., Goldberg, M. D., Kalnay, E., McMillin, L. M., Revercomb, H., Rosenkranz, P. W., Smith, W. L., Staelin, D. H., Strow, L. L., and Susskind, J.: AIRS/AMSU/HSB on the Aqua mission: Design, science objectives, data products, and processing systems, IEEE T. Geosci. Remote, 41, 253–264, 2003. 24674

Baran, A. J. and Francis, P. N.: On the radiative properties of cirrus cloud at solar and thermal wavelengths: A test of model consistency using high-resolution airborne radiance measurements, Q. J. Roy. Meteor. Soc.,130, 763–778, 2004. 24676

Baran, A. : On the scattering and absorption properties of cirrus cloud, J. Quant. Spectrosc. Ra., 89, 17–36, 2004.

Baran, A. J., Connolly, P. J., and Lee, C.: Testing an ensemble model of cirrus ice crystals using

midlatitude in situ estimates of ice water content,volume extinction coefficient and the total solar optical depth, J. Quant. Spectrosc. Ra., 110, 1579–1598, 2009.. 24692

Boehm, M. T. and Lee., S.: The Implications of Tropical Rossby Waves for Tropical Tropopause Cirrus Formation and for the Equatorial Upwelling of the BrewerDobson Circulation, J. Atmos Sci., 60, 247–261, 2003. 24673

Bony, S. and Emanuel, K. A.: A Parameterization of the Cloudiness Associated with Cumulus Convection; Evaluation Using TOGA COARE Data, J. Atmos Sci., 58, 3158–3183, 2001. 24673

Boudala, F. S., Isaac, G. A., Fu, Q., and Cober, S. G.: Parameterization of effective ice particle size for high-latitude clouds, Int. J. Climatol., 22, 1267–1284, 2002. 24673, 24692

Chahine, M. T., Pagano, T. S., Aumann, H. H., Atlas, R., and Coauthors: AIRS: Improving weather forecasting and providing new data on greenhouse gases, B. Am. Meteor. Soc., 87, 911–926, 2006. 24674

Chédin, A., Scott, N. A., Wahiche, C., and Moulinier, P.: The improved initialization inversion method: A high resolution physical method for temperature retrievals from satellites of the TIROS-N series, J. Clim. Appl. Meteor., 24, 128–143, 1985. 24674

Chepfer, H., Bony, S., Winker, D., Cesana, G., Dufresne, J. L., Minnis, P., Stubenrauch, C. J., and Zeng, S.: The GCM-Oriented CALIPSO Cloud Product (CALIPSO-GOCCP), J. Geophys. Res., 115, D00H16, doi:10.1029/2009JD012251, 2010. 24672

Chevallier, F., Cheruy, F., Scott, N. A., and Chedin, A.: A neural network approach for a fast and accurate computation of longwave radiative budget, J. Appl. Meteorol., 37, 1385–1397, 1998. 24674

Chung, S. G., Ackerman, S. A., Van Delst, P. F., and Menzel, W. P.: Model Calculations and Interferometer Measurements of Ice- Cloud Charancterics, J. Appl. Meteorol., 39, 634–644, 2000. 24673

Donner, L. J., Seman, C. J., Soden, B. J., Hemler, R. S., and Warren, J. C. : Large-scale ice clouds in the GFDL SKYHI general circulation model, J. Geophys. Res., 102, 745–768, 1997. 24673

Doutriaux-Boucher, M.: Evaluation of cloud thermmodynamic phase parametriization in the LMDZ GCM by using POLDER staellite data, Geophys. Res. Lett., 31, L06126, doi:10.1029/2003GL019095, 2004

Edwards, J. M., Havemann, S., Thelen, J.-C. and Baran, A. J.: A new parametrization for the radiative properties of ice crystals: Comparison with existing schemes and impact in a GCM,

Atmos. Res., 83, 19–35, 2007. 24673, 24692

Field, P. R., Hogan, R. J., Brown, P. R., Illingworth, A. J., Choularton, T. W., and Cotton, R. J.: Parametrization of ice-particle size distributions for mid-latitude stratiform cloud, Q. J. Roy. Meteorol. Soc., 131, 1997-2017, 2005.

Field, P. R., Heymsfield, A. J., and Bansemer, A.: Shattering and Particle Interarrival Times Measured by Optical Array Probes in Ice Clouds, J. Atmos. Oceanic Technol., 23, 1357–1371, 2006. 24673

Field, P. R. and Wood, R.: Precipitation and Cloud Structure in Midlatitude Cyclones, J. Climate, 20, 233–254, doi:10.1175/2007JAS2344.1, 2007.

Francis, P. N. and Foot, J. S.: Aircraft measurements of the solar and infrared radiative properties of cirrus and their dependence on ice crystal shape, J. Geophys. Res., 104, 685–695, 1999. 24687

Garrett, T. J., Heymsfield, A. J., McGill, M. J., Ridley, B. A., Baumgardner, D. G., Bui, T. P. and Webster, C. R.: Convective generation of cirrus near the tropopause, J. Geophys. Res.,109, D21203, doi:10.1029/2004JD004952, 2004 24673, 24693

Gayet, J.-F., Mioche, G., Shcherbakov, V., Gourbeyre, C., Busen, R., and Minikin, A.: Optical properties of pristine ice crystals in mid-latitude cirrus clouds: a case study during CIRCLE-2 experiment, Atmos. Chem. Phys., 11, 2537–2544, doi:10.5194/acp-11-2537-2011, 2011. 24687

Giraud, V., Thouron, 0., Riedi, J., and Goloub, P.: Analysis of direct comparison of cloud top temperature and infrared split window signature against independant retrievals of cloud thermodynamic phase, Geophys. Res. Lett., 28, 983–986, 2001

Heymsfield, A. J., and Platt, C. M. R.: A Parameterization of the Particle Size Spectrum of Ice Clouds in Terms of the Ambient Temperature and the Ice Water Content, J. Atmos. Sci., 41, 846–855, 1984. 24673

Heymsfield, A. J., Matrosov, S., Baum, B.: Ice Water Path-optical Depth ReLationships for Cirrus and Deep stratiform ice cloud layers, J. Appl. Meteorol., 42, 1369–1387

Heymsfield, A. J.: Properties of Tropical and Midlatitude Ice Cloud Particle Ensembles. Part II: Applications for Mesoscale and Climate Models, J. Atmos. Sci., 60, 2592–2611, 2003. 24693

Hong, G., Yang, P., Gao, B.-C., Baum, B. A., Hu, Y. X., King, M. D., and Platnik, S.: High Cloud Properties from Three Years of MODIS Terra and Aqua Collection-4 Data over the Tropics, J. Appl. Meteorol. Clim., 46,1840–1856, 2007. 24673

Hu, Y. and Winker, D.: Caliop Cloud Phase Discrimination Algorithm, J. Atmos. Oceanic Tech-

**Bulk microphysical properties of semi transparent cirrus from AIRS**

A. Guignard et al.

Title Page

| Abstract | Introduction |
| Conclusions | References |
| Tables | Figures |

◄◄   ►►

◄   ►

Back   Close

Full Screen / Esc

Printer-friendly Version

Interactive Discussion

nol., 26, 2293–2309, doi:10.1175/2009JTECHA1280.1, 2009. 24685

Ivanova, D., Mitchell, D. L., Arnotta, W. P. and Poellotb, M.: A GCM parameterization for bimodal size spectra and ice mass removal rates in mid-latitude cirrus clouds, Atmos. Res., 59–60, 89–113, 2001. 24673, 24692

5  Kahn, B. H., Eldering, A., Ghil, M., Bordoni, S., and Clough, S. A.: Sensitivity Analysis of Cirrus Cloud Properties from High-Resolution Infrared Spectra. Part I: Methodology and Synthetic Cirrus, J. Climate, 17, 4856–4870, 2004. 24673

Kahn, B. H., Eldering, A., Braverman, A. J., Fetzer, E. J., Jiang, J. H., Fishbein, E., and Wu, D. L.: Toward the characterization of upper tropospheric clouds using Atmospheric In-

10  frared Sounder and Microwave Limb Sounder observations, J. Geophys. Res., 112, D05202, doi:10.1029/2006JD007336, 2007. 24673

Kahn, B. H., Liang, C. K., Eldering, A., Gettelman, A., Yue, Q., and Liou, K. N.: Tropical thin cirrus and relative humidity observed by the Atmospheric Infrared Sounder, Atmos. Chem. Phys., 8, 1501–1518, doi:10.5194/acp-8-1501-2008, 2008. 24673, 24679

15  Korolev, A. and Isaac, G.: Roundness and aspects ratios of particles in ice clouds, J. Atmos, 60, 1795–1808, 2003. 24685, 24687

Korolev, A. V., Isaac, G. A., Mazin, I. P. and Barker, H. W.: Microphysical properties of continental clouds from in-situ measurements, Q. J. Ro. Meteor. Soc., 127, 2117-2151, 2001. 24673, 24691, 24693

20  Korolev, A. V. and Isaac, G. A: Shattering during Sampling by OAPs and HVPS. Part I: Snow Particles, J. Atmos. Ocean Technol., 22, 528–542, 2004. 24673

L'Ecuyer, T. S., Gabriel, P., Leesman, K., Cooper, S. J., and Stephens, G. L.: Objective assessment of the information content of visible and infrared radiance measurements for cloud microphysical property retrievals over the global oceans. Part I: Liquid clouds, J. Appl. Me-

25  teor. Climatol., 45, 20–41, 2006. 24679

Luo, Z. and Rossow, W. B. : Characterizing Tropical Cirrus Life Cycle, Evolution, and Interaction with Upper-Tropospheric Water Vapor Using Lagrangian, J. Climate, 17, 4541–4563, 2004. 24673

Lynch, D. K., Sassen, K., Starr, D. O. C., and Stevens, G., Cirrus, 480 pp., Oxford Univ. Press,

30  New York, USA, 480 pp., 2002.

Mace, G. G., Sassen, K., Kinne, S., and Ackerman, T. P.: An examinationo f cirrus cloud characteristicsu singd ata from millimeter wave radar and lidar: The 24 April SUCCESS casestudy, Geophys. Res. Lett., 25, 1133–1136, 1998.

**Bulk microphysical properties of semi transparent cirrus from AIRS**

A. Guignard et al.

Mace, G. G., Zhang, Q., Vaughan, M., Marchand, R., Stephens, G., Trepte, C., and Winker, D.: A description of hydrometeor layer occurrence statistics derived from the first year of merged Cloudsat and CALIPSO data, J. Geophys. Res., 114, D00A26, doi:10.1029/2007JD009755, 2009. 24680

Martins, E., Noel, V. and Chepfer, H.: Properties of cirrus and subvisible cirrus from nighttime Cloud-Aerosol Lidar with Orthogonal Polarization (CALIOP), related to atmospheric dynamics and water vapor, J. Geophys. Res., 116, D02208, doi:10.1029/2010JD014519, 2011. 24685

Mc Farquhar, G. and Heymsfield, A. J.: Microphysical characteristics of three anvils sampled during the Central Equatorial Pacific experiment, J. Atmos. Sci, 53, 2401–2423, 1996.

Mc Farquhar, G., Heymsfield, A. J.: Parameterization of Tropical Cirrus Ice Crystal Size Distributions and Implications for Radiative Transfer: Results from CEPEX, J. Atmos. Sci., 54, 2187–220,1997.

Mc Farquhar, G. and Heymsfield, A. J. : The Definition and Significance of an Effective Radius for Ice Clouds, J. Atmos. Sci., 55, 2039–2052, 1997. 24677

Mc Farquhar, G., Iacobellis, S. and Somerville C. J.: SCM Simulations of Tropical Ice Clouds Using Observationally Based Parameterizations of Microphysics, J. Climate, 16, 1643–1664, 2003. 24673, 24693, 24725

Mc Farquhar, G., Um, J., Freer, M., Baumgardner, D., Kok, G. L., and Mace, G.: Importance of small ice crystals to cirrus properties: Observations from the Tropical Warm Pool International Cloud Experiment (TWP-ICE), Geophys. Res. Lett., 34, L13803, doi:10.1029/2007GL029865, 2007. 24673

McFarlane, N. A., Boer, G. J., Blanchet, J.-P., and Lazare, M.: The canadian climate Centre second-generation general circulation model and its equilibrium climate, J. Climate, 5, 1013–1044, 1992. 24673

Mitchell, D. L., Chai, S. K., and Liu, Y.: Modeling cirrus clouds, I. Treatment of bimodal size spectra and case study analysis, J. Atmos. Sci., 53, 2952–2966, 1996. 24676, 24677, 24689, 24691

Mitchell, D. L., Macke, A., and Liu, Y.: Modeling cirrus clouds, II, Treatment of radiative properties, J. Atmos. Sci., 53, 2967–2988, 1996.

Mitchell, D. L. and Baran, A. J.: Testing of the modified anomalous diffraction approximation with T-matrix calculations for hexagonal columns, Twelfth ARM Science Team Meeting Proceedings, St. Petersburg, Florida, 8–12 April, 2002 24677

**Bulk microphysical properties of semi transparent cirrus from AIRS**

A. Guignard et al.

Title Page

Abstract | Introduction

Conclusions | References

Tables | Figures

◄ | ►

◄ | ►

Back | Close

Full Screen / Esc

Printer-friendly Version

Interactive Discussion

Mitchell, D.: Effective Diameter in Radiation Transfer: General Definition, Applications and Limitations, J. Atmos. Sci., 59, 2330–2346, 2002.

Mitchell, D. L., Baran, A. J., Arnott, W. P., and Schmitt, C.: Testing and comparing the modified anomalous diffraction approximation, J. Atmos. Sci., 63, 2948–2962, 2006.

Mitchell, D. L.: Inferring cirrus size distributions through satellite remote sensing and microphysical databases, J. Atmos. Sci., 67, 1106–1125, 2009. 24687

Mitchell, D. L., Lawson, R. P., and Baker, B.: Understanding effective diameter and its application to terrestrial radiation in ice clouds, Atmos. Chem. Phys., 11 3417–3428, 2011. 24677

Péquignot, E., Céhdin, A., and Scott, N. A.: Infrared continental surface emissivity spectra retrieved from AIRS hyperspectral sensor, J. Appl. Meteor. Climatol., 47, 1619–1633, 2008. 24675

Platnick, S., King, M. D., Ackerman, S. A., Menzel, W. P., Baum, B. A., Ridi, J. C., and Frey, R. A.: The MODIS Cloud Products: Algorithms and Examples From Terra, IEEE T. Geosci. Remote, 41, 459–473, 2003. 24673

Pierangelo, C., Mishchenko, M., Balkanski, Y., and Céhdin, A.: Retrieving the effective radius of Saharan dust coarse mode from AIRS, Geophys. Res. Lett., 32, L20813, doi:10.1029/2005GL023425, 2005. 24677

Rädel, G., Stubenrauch, C.J., Holtz, R.: Retrieval of effective ice crystal size in the infrared: Sensitivity study and global measurments from TIROS-N Operationnal Vertical Sounder. J. Geophys. Res., 108, D9, 4281, doi:10.1029/2002JD002801, 2003108, 2003. 24673, 24677, 24678, 24682, 24684, 24689, 24690, 24694

Riedi, J., Marchant, B., Platnick, S., Baum, B. A., Thieuleux, F., Oudard, C., Parol, F., Nicolas, J.-M., and Dubuisson, P.: Cloud thermodynamic phase inferred from merged POLDER and MODIS data, Atmos. Chem. Phys., 10, 11851–11865, doi:10.5194/acp-10-11851-2010, 2010. 24685

Roebeling, R. A., Feijt, A. J., and Stammes, P.: Cloud property retrievals for climate monitoring: Implications of differences between Spinning Enhanced Visible and Infrared Imager (SEVIRI) on METEOSAT-8 and Advanced Very High Resolution Radiometer (AVHRR) on NOAA-17, J. Geophys. Res., 111, D20210, doi:10.1029/2005JD006990, 2006. 24673

Rossow, W. B. and Schiffer, R. A.: Advances in understanding clouds from ISCCP, B. Am. Meteor. Soc., 80, 2261–2287, 1999. 24683

Sassen, K. and Dodd, G. C.: Homogeneous nucleation rate for highly supercooled cirrus cloud droplets, J. Atmos. Sc., 45, 1357–1369, 1988.

Scott, N. A., and Chedin, A.: A fast line-by-line method for atmospheric absorption computations: the 4A Automized Atmospheric Absorption Atlas, J. Appl. Meteorol., 20, 801–812, 1981. 24677

Seemann, S. W., Borbas, E. E., Knuteson, R. O., Stephenson, G. R., and Huang, H. L.: Development of a Global Infrared Land Surface Emissivity Database for Application to Clear Sky Sounding Retrievals from Multispectral Satellite Radiance Measurements. J. Appl. Meteor. Climatol., 47, 108–123, doi:10.1175/2007JAMC1590.1, 2008. 24675

Seo, E. K. and Liu, G.: Determination of 3D cloud ice water contents by combining multiple data sources from satellite, ground radar, and a numerical model, J. Appl. Metorol., 45, 1494–1504, 2006. 24692

Stamnes, K., Tsay, S. , Wiscombe, W. and Jayaweera, K.: Numerically stable algorithm for discrete-ordinate-method radiative transfer in multiple scattering and emitting layered media, Appl. Optics, 27, 2502–2509, 1988. 24677

Stith, J. L., Dye, A. E., Bansemer, A., and Heymsfield J. A.: Microphysical Observations of Tropical Clouds, J. Appl. Metorol., 41, 97–117, 2002. 24673

Stephens, G. L., Vane, D. G., Boain, R. J., Mace, G. G., Sassen, K., Stephens, G. L., Vane, D. G., Boain, R. J., Mace, G. G., Sassen, K., Wang, Z., Illingworth, A. J., O'Connor, E. J., Rossow, W. B., and Durden, S. L.: The CloudSat mission and the A-train, Am. Meteorol. Soc., 83, 1771-1790, 2002. 24680

Stubenrauch, C. J., Holz, R., Chédin, A., Mitchell, D. L., and Baran, A. J : Retrieval of cirrus ice crystal sizes from 8.3 and 11.1 $\mu m$ emissivities determined by the improved initialization inversion of TIROS-N Operational Vertical Sounder observations, J. Geophys. Res., 104, 793–808 1999. 24673

Stubenrauch, C. J., Eddounia, F., and Rädel, G.: Correlations between microphysical properties of large-scale semi-transparent cirrus and the state of the atmosphere, Atmos. Res., 72, 403–423, 2004. 24689

Stubenrauch, C. J., Chédin, A., Rädel, G., Scott, N. A., and Serra, S.: Cloud Properties and Their Seasonal and Diurnal Variability from TOVS Path-B, J. Climate, 19, 5531–5553 2006. 24672

Stubenrauch, C. J., Eddouina, F., Edwards, J. M., and Macke, A.: Evaluation of Cirrus Parameterizations for Radiative Flux Computations in Climate Models Using TOVSScaRaB Satellite Observations, J. Climate, 20, 4459–4475, doi:10.1175/JCLI4251.1, 2007. 24691

Stubenrauch, C. J., Cros, S., Lamquin, N., Armante, R., Chédin, A., Crevoisier, C., and Scott,

N. A.: Cloud properties from AIRS and evaluation with CALIPSO, J. Geophys. Res., 113, D00A10, doi:10.1029/2008JD009928, 2008. 24676

Stubenrauch, C. J., Cros, S., Guignard, A., and Lamquin, N.: A 6-year global cloud climatology from the Atmospheric InfraRed Sounder AIRS and a statistical analysis in synergy with CALIPSO and CloudSat, Atmos. Chem. Phys., 10, 7197–7214, doi:10.5194/acp-10-7197-2010, 2010. 24672, 24673, 24675, 24676, 24680

Susskind, J., Barnet C., and Blaisdell J.: Retrieval of atmospheric and surface parameters from AIRS/AMSU/HSB data in the presence of clouds, IEEE Trans. Geosci. Remote Sens., 41, 390–409, 2003. 24674

Susskind, J., Barnet, C., Blaisdell, J., Iredell, L., Keita, F., Kouvaris, L., Molnar, G., and Chahine, M.: Accuracy of geophysical parameters derived from AIRS/AMSU as a function of fractional cloud cover, J. Geophys. Res., 111, D09S17, doi:10.1029/2005JD006272, 2006. 24674

Wang, J., Rossow, W. B., and Zhang, Y.: Cloud Vertical Structure and its Variations from a 20-Yr Global Rawinsonde Dataset, J. Climate, 13, 3041–3056, 2000. 24688

Winker, D. M. and Pelon, J. R. and McCormick, M. P.: The CALIPSO mission: Spaceborne lidar for observation of aerosols and clouds, Proc. SPIE 4893, Lidar Remote Sensing for Industry and Environnment III, 1–11, doi:10.1117/12.466539, 2003. 24680

Winker, D. M., Hunt, W. H., and McGill, M. J.:Initial performance assessment of CALIOP, Geophys. Res. Lett., 34, L19803, doi:10.1029/2007GL030135, 2007. 24679

Winker, D., Getzewitch, B., and Vaughan, M.: Evaluation and Applications of Cloud Climatologies from CALIOP, Proc. Int. Laser Radar Conference (ILRC), 2008.

Winker, D. M., Vaughan, M. A., Omar, A., Hu, Y., and Powell, K. A.:Overview of the CALIPSO mission and CALIOP data processing algorithms, J. Atmos. Ocean. Technol., 26, 2310–2323, 2009. 24679

Wylie, D. and Menzel, W. P: Four Years of Global Cirrus Cloud Statistics Using HIRS, J. Climate, 7, 1972–1986, 1994. 24673

Wylie, D. and Menzel, W. P: Eight Years of High Cloud Statistics Using HIRS, J. Climate, 12, 170–184, 1999. 24672

Wylie, D., Jackson, D. L., Menzel, W. P., Bates, J. J.: Trends in Global Cloud Cover in Two Decades of HIRS Observations, J. Climate, 18, 3021–3031, 2005. 24672

Yang, P., Weia, H.-L., and Baumb, B. A.:The spectral signature of mixed-phase clouds composed of non-spherical ice crystals and spherical liquid droplets in the terrestrial window region, J. Quant. Spectrosc. Ra., 79, 1171–1188, 2002. 24685

**Bulk microphysical properties of semi transparent cirrus from AIRS**

A. Guignard et al.

Title Page

Abstract | Introduction

Conclusions | References

Tables | Figures

|◄ | ►|

◄ | ►

Back | Close

Full Screen / Esc

Printer-friendly Version

Interactive Discussion

Yue, Q., Liou, K. N., Ou, S. C., Kahn, B. H., Yang, P., and Mace, G.: Interpretation of AIRS data in thin cirrus atmospheres based on a fast radiative transfer model, J. Atmos. Sci., 64, 3827–3842, 2007.

Yue, Q. and Liou, K. N.: Cirrus cloud optical and microphysical properties determined from AIRS infrared spectra, Geophys. Res. Lett., 36, L05810, doi:10.1029/2008GL036502, 2009.

**Bulk microphysical properties of semi transparent cirrus from AIRS**

A. Guignard et al.

Back          Close

Full Screen / Esc

Printer-friendly Version

Interactive Discussion

Discussion Paper | Discussion Paper | Discussion Paper | Discussion Paper | Discussion Paper

**Bulk microphysical properties of semi transparent cirrus from AIRS**

A. Guignard et al.

**Table 1.** Compilation of Uncertainty Sources and their Influence on the Retrieval of the Mean Ice-Crystal Diameter $D_e^a$. Thin clouds correspond to $\epsilon \approx 0.35$ and thick clouds to $\epsilon \approx 0.76$.

| | $(D_e^{std} - D_e'^{std})/D_e^{std}$ | | | |
| | Thin clouds | | Thick clouds | |
| | 15 µm | 60 µm | 15 µm | 60 µm |
|---|---|---|---|---|
| $\Delta Z_{cld} = +1\,$km | +1 % | −1 % | 0 % | −1 % |
| $\Delta h_{cld} = +4\,$km | +2 % | −1 % | −1 % | −3 % |
| Lapse Rate ($6.5 \rightarrow 11.5\,°$C km$^{-1}$) | +6 % | −2 % | −1 % | −1 % |
| $\Delta T_s = -15\,$K | +1 % | −1 % | −2 % | −3 % |
| complex shape → pristine shape | +1 % | +2 % | +6 % | +2 % |
| SSP (Baran → Mitchell) | −2 % | −2 % | −1 % | −1 % |

**Table 2.** Statistical analysis of the effect of cuts: percentage of cirrus kept with cuts on cloud top temperature and on cloud emissivity in three latitude bands (NH:45° N–60° N,Trop: 15° N–15° S, SH:45° S–60° S), for boreal winter and boreal summer and over different surfaces (ocean, land and all surfaces).

| | Ocean | | Land | | All | |
|---|---|---|---|---|---|---|
| | DJF | JJA | DJF | JJA | DJF | JJA |
| $T_{cld} \leq 230\,K$ | | | | | | |
| NH mid-latitudes | 63 % | 18 % | 59 % | 28 % | 62 % | 23 % |
| Tropics | 59 % | 55 % | 46 % | 51 % | 55 % | 51 % |
| SH mid-latitudes | 20 % | 66 % | 42 % | 73 % | 21 % | 66 % |
| $0.2 \leq \epsilon_{cld} \leq 0.85$ | | | | | | |
| NH mid-latitudes | 70 % | 69 % | 79 % | 69 % | 73 % | 69 % |
| Tropics | 66 % | 67 % | 71 % | 70 % | 68 % | 68 % |
| SH mid-latitudes | 64 % | 73 % | 74 % | 75 % | 64 % | 73 % |

**Table 3.** Relative cloud amount of HC and ST-HIC over the period 2003-2009 in three latitude bands (NH:45° N–60° N, Trop:15° N–15° S, SH:45° S–60° S), for boreal winter and boreal summer and over different surfaces (ocean, land and all surfaces).

|  | Ocean | | Land | | All | |
|---|---|---|---|---|---|---|
|  | DJF | JJA | DJF | JJA | DJF | JJA |
| **High clouds** | | | | | | |
| NH mid-latitudes | 26 % | 26 % | 43 % | 37 % | 29 % | 32 % |
| Tropics | 64 % | 59 % | 70 % | 62 % | 65 % | 60 % |
| SH mid-latitudes | 10 % | 25 % | 29 % | 51 % | 11 % | 25 % |
| **Ci-ST** | | | | | | |
| NH mid-latitudes | 7 % | 1 % | 15 % | 3 % | 9 % | 2 % |
| Tropics | 18 % | 15 % | 16 % | 12 % | 17 % | 15 % |
| SH mid-latitudes | 1 % | 8 % | 5 % | 19 % | 1 % | 8 % |

Title Page

Abstract | Introduction

Conclusions | References

Tables | Figures

◄◄ | ►►

◄ | ►

Back | Close

Full Screen / Esc

Printer-friendly Version

Interactive Discussion

**Bulk microphysical properties of semi transparent cirrus from AIRS**

A. Guignard et al.

**Table 4.** ST-HIC mean properties and medians of bulk microphysical properties over the period 2003–2009, in three latitude bands (NH:45° N–60° N, Trop: 15° N–15° S, SH: 45° S–60° S), for boreal winter and boreal summer and over different surfaces (ocean, land and all surfaces).

| | $\epsilon_{cld}$ | | $T_{cld}$ (K) | | $\Delta Z(km)$ | | % SL | | $D_e(\mu m)$ | | IWP ($g\,m^{-2}$) | | Agg(%) | | % $D_{>}85\mu m$ | |
|---|---|---|---|---|---|---|---|---|---|---|---|---|---|---|---|---|
| | DJF | JJA | DJF | JJA | DJF | JJA | DJF | JJA | DJF | JJA | DJF | JJA | DJF | JJA | DJF | JJA |
| Ocean | | | | | | | | | | | | | | | | |
| NH mid-latitudes | 0.57 | 0.47 | 222 | 224 | 4.0 | 3.4 | 52 | 41 | 57 | 54 | 26 | 16 | 50 | 53 | 15 | 5 |
| Tropics | 0.49 | 0.49 | 217 | 217 | 4.2 | 3.9 | 50 | 48 | 51 | 54 | 19 | 20 | 56 | 56 | 2 | 4 |
| SH mid-latitudes | 0.57 | 0.61 | 225 | 221 | 3.7 | 4.1 | 48 | 49 | 46 | 54 | 18 | 30 | 56 | 62 | 4 | 10 |
| Land | | | | | | | | | | | | | | | | |
| NH mid-latitudes | 0.57 | 0.51 | 220 | 223 | 4.1 | 3.3 | 67 | 62 | 50 | 53 | 23 | 18 | 41 | 39 | 3 | 1 |
| Tropics | 0.52 | 050 | 218 | 218 | 4.2 | 3.7 | 51 | 48 | 52 | 53 | 21 | 20 | 44 | 45 | 2 | 2 |
| SH mid-latitudes | 0.57 | 0.58 | 221 | 219 | 3.1 | 2.9 | 76 | 58 | 29 | 44 | 13 | 20 | 53 | 46 | 1 | 2 |
| All | | | | | | | | | | | | | | | | |
| NH mid-latitudes | 0.57 | 0.49 | 221 | 224 | 4.1 | 3.3 | 62 | 55 | 54 | 53 | 25 | 17 | 48 | 44 | 12 | 5 |
| Tropics | 0.50 | 0.49 | 217 | 217 | 4.2 | 3.9 | 50 | 48 | 51 | 54 | 19 | 20 | 53 | 54 | 3 | 4 |
| SH mid-latitudes | 0.57 | 0.61 | 224 | 221 | 3.7 | 4.1 | 49 | 49 | 45 | 54 | 18 | 30 | 56 | 61 | 4 | 10 |
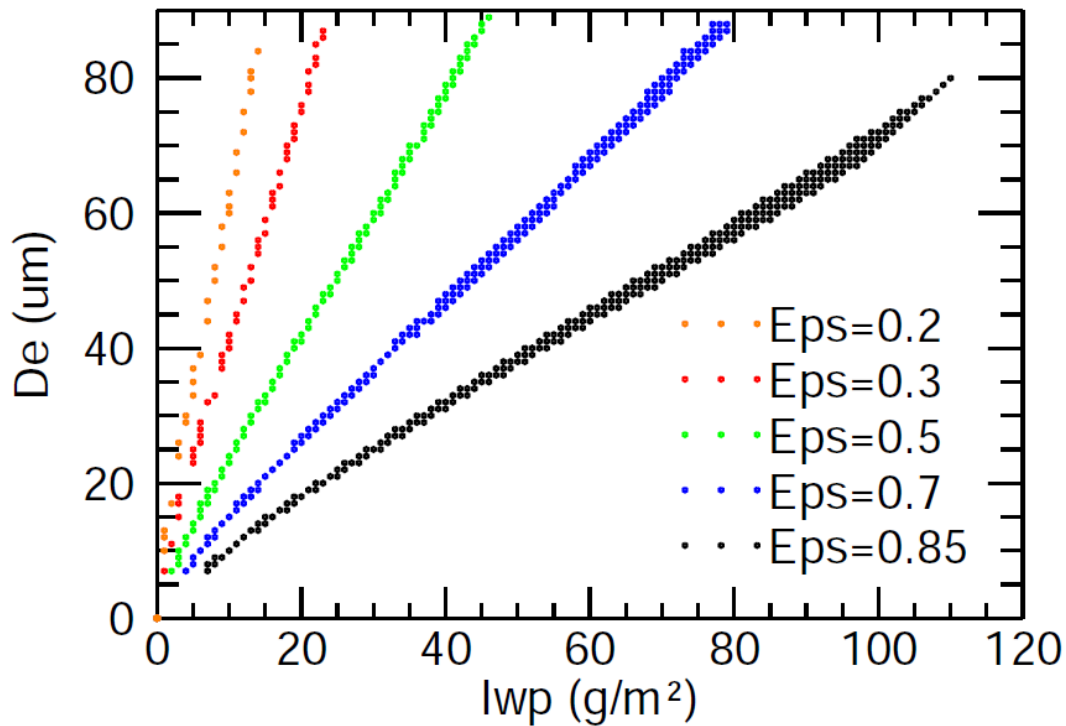
**Fig. 1.** Effective ice crystal diameter as a function of ice water path. Each color corresponds to a different value of the effective cloud emissivity whose value is indicated.

**Fig. 2.** Normalized emissivity difference as a function of wavelength, separately for aggregate-like and column-like ice crystal shape, full lines and broken lines, respectively. Results are shown for two values of IWP, $10\,\mathrm{g\,m^{-2}}$ (top) and $20\,\mathrm{g\,m^{-2}}$ (bottom) and three effective ice crystal diameters (10, 30, 50 μm, red, green and blue, respectively). The six channels selected for the retrieval are marked with black squares.
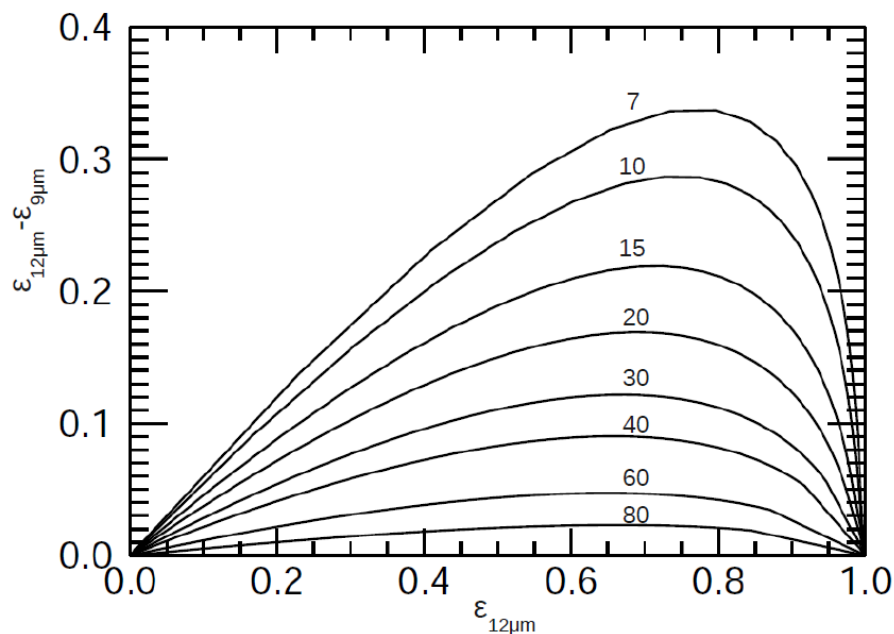
**Fig. 3.** Effective emissivity differences $\Delta\varepsilon_{12\mu m} - \varepsilon_{9\mu m}$ as a function of $\varepsilon_{12\mu m}$ assuming aggregate-like ice crystal shape. Each line corresponds to a different effective diameter $D_e$, which value is indicated in µm.

Full Screen / Esc

Printer-friendly Version

Interactive Discussion
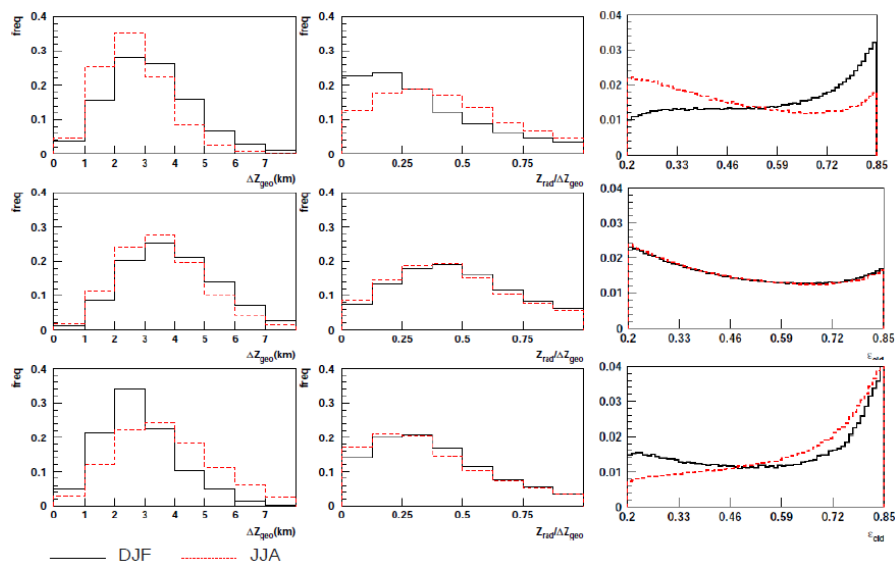


**Fig. 4.** seasonal distributions of geometrical thickness (on the left side ) and the ratio between apparent and geometrical thickness (on the right side) in three latitude bands in boreal winter and summer (black lines and red lines respectively over the peiod 2007–2008.

Title Page

Abstract | Introduction

Conclusions | References

Tables | Figures

|◄ | ►|

◄ | ►

Back | Close

Full Screen / Esc

Printer-friendly Version

Interactive Discussion
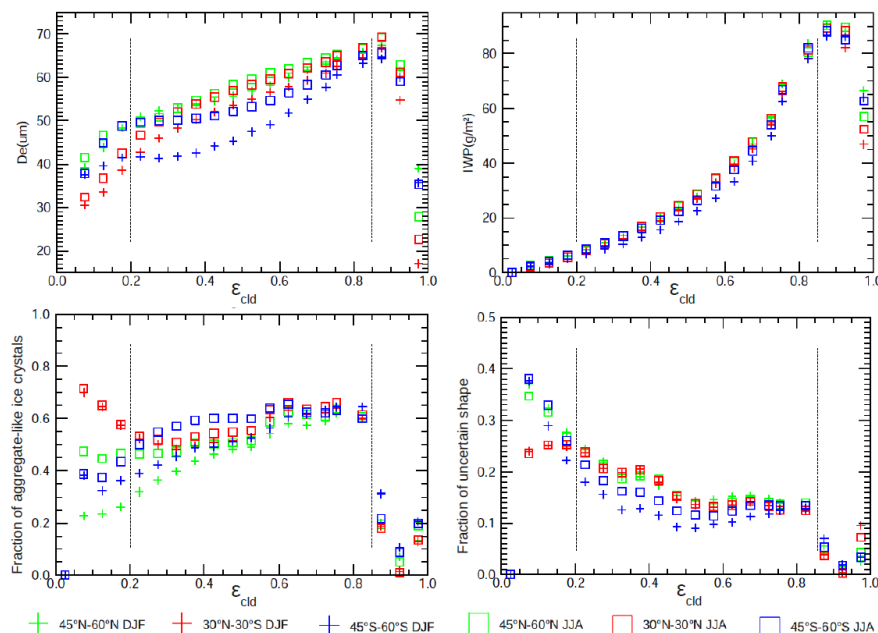


**Fig. 5.** Average bulk microphysical properties as a function of cloud effective emissivity from 2004 to 2009. Crosses and squares represent averages over DJF and JJA, respectively. Green symbols are for NH mid-latitudes, red for the tropics and blues for SH mid-latitudes.
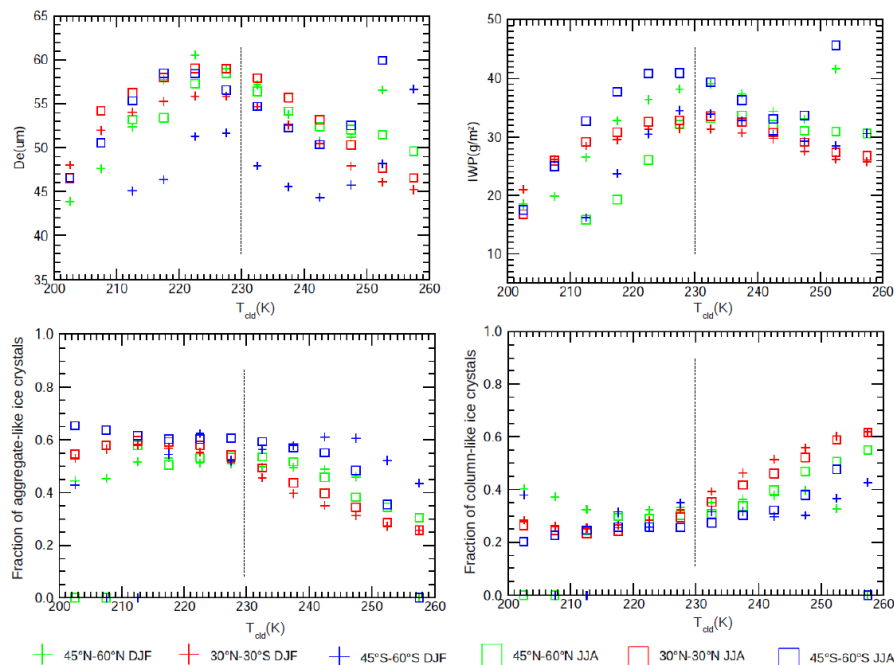
**Fig. 6.** Average bulk microphysical properties as a function of cloud temperature from 2004 to 2009. Crosses and squares represent averages over DJF and JJA, respectively. Green symbols are for NH mid-latitudes, red for the tropics and blues for SH mid-latitudes.
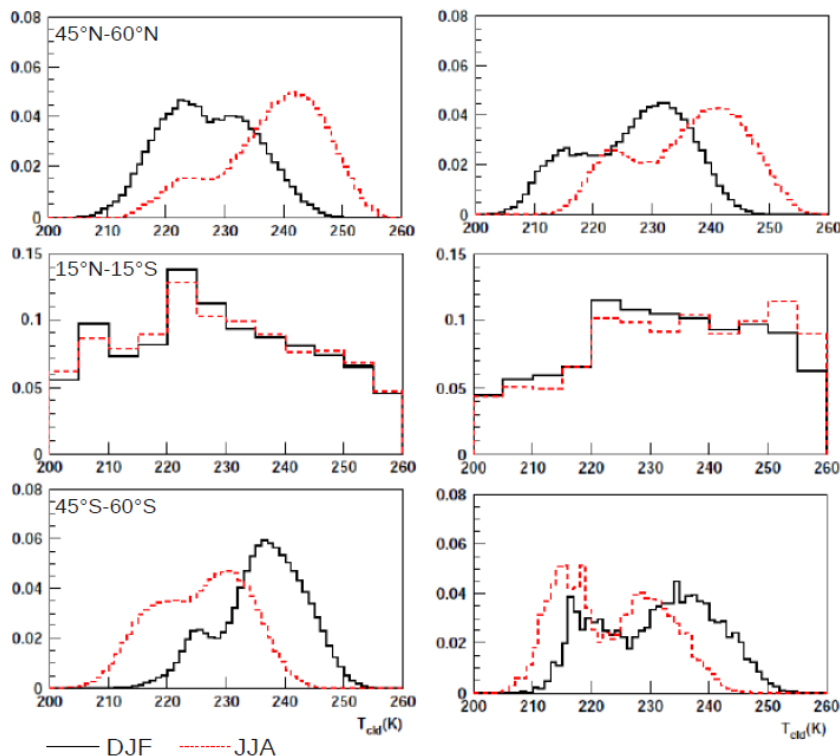
**Fig. 7.** Zonal distributions of cloud temperature used to define semi-transparent cirrus over ocean (left) and over land (right) from 2003 to 2009. Latitude bands are defined on the top left corner of the right hand side figures. Boreal winter and summer are represented in black and red, respectively.

Title Page

Abstract | Introduction

Conclusions | References

Tables | Figures

|◄ | ►|

◄ | ►

Back | Close

Full Screen / Esc

Printer-friendly Version

Interactive Discussion
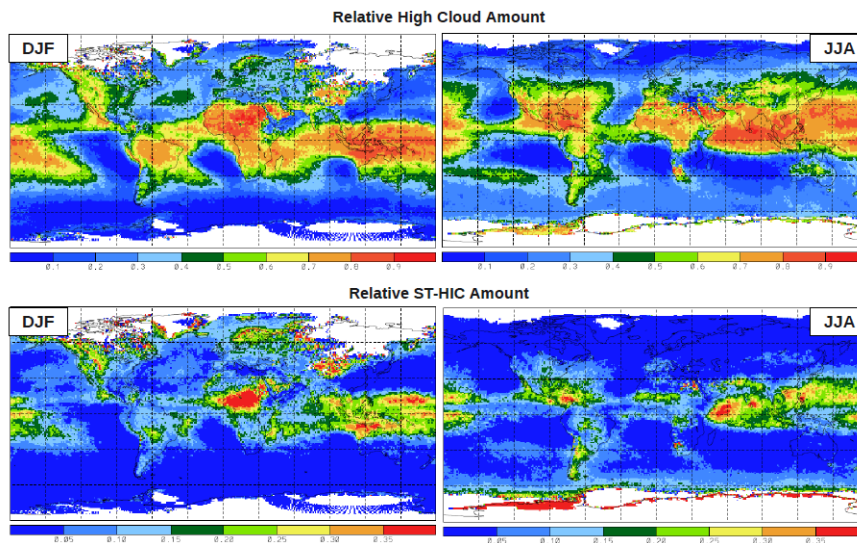


**Fig. 8.** Relative high cloud amount and relative semi-transparent high ice cloud amount (top and bottom respectively) for boreal winter and boreal summer (left hand side and right hand side figures, respectively) over the period 2003–2009.
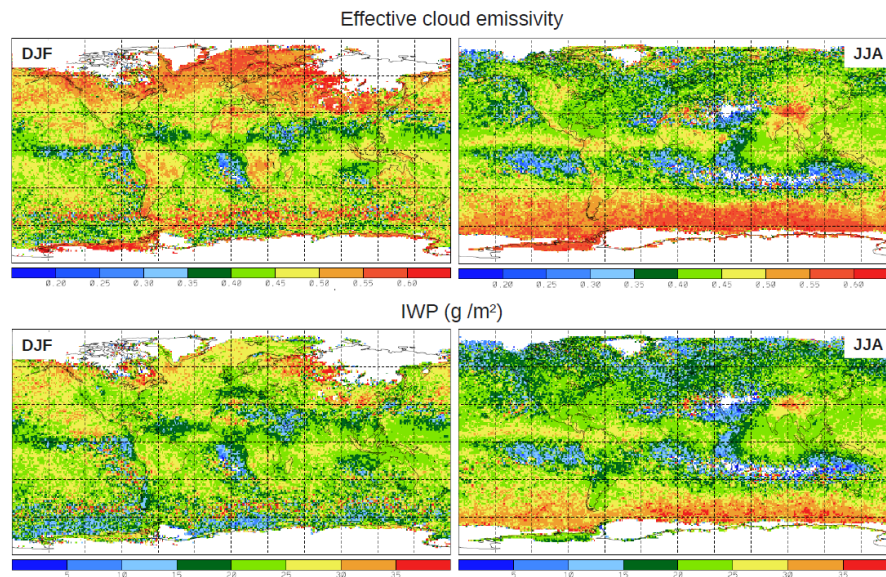
**Fig. 9.** Cloud effective emissivity and Ice Water Path (top and bottom figure respectively) for boreal winter and boreal summer (right hand side and left hand side figures, respectively) over the period 2003–2009.
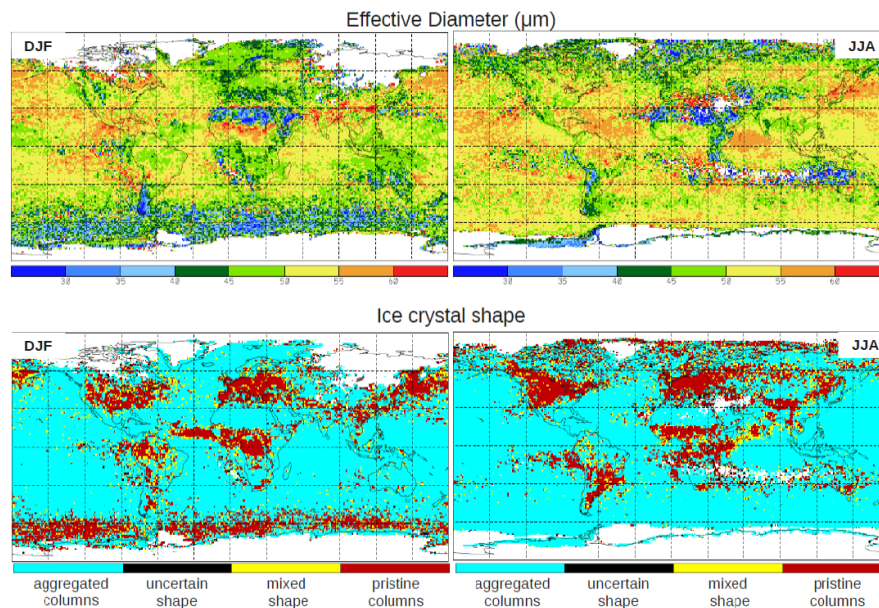
**Fig. 10.** Effective diameter and shape of ice crystal (top and bottom figure respectively) for boreal winter and boreal summer (right hand side and left hand side figures, respectively) over the period 2003–2009.

Full Screen / Esc

Printer-friendly Version

Interactive Discussion
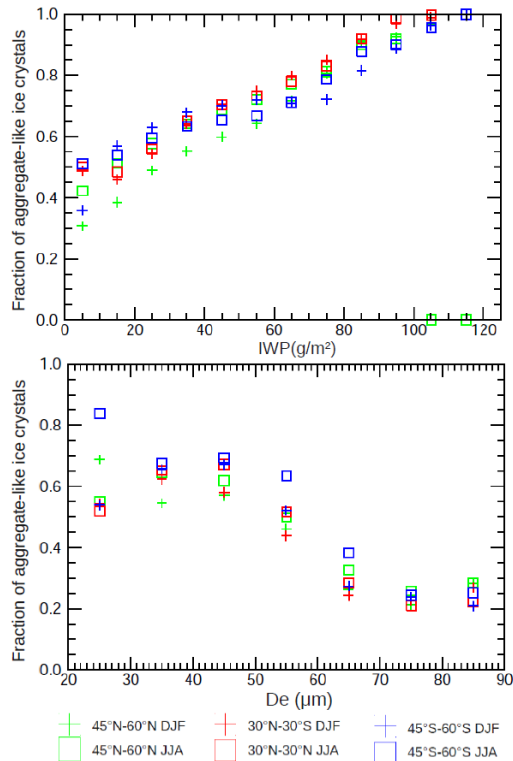


**Fig. 11.** Correlation of Ice Water Path and effective diameter with the fraction of aggregated-like crystals (top and bottom respectively), from 2003 to 2009 over ocean separately for boreal winter and boreal summer. Cross and squares represent averages over DJF and JJA, respectively. Green symbols are for northern mid-latitudes, red for the tropics and blue for the southern mid-latitudes.
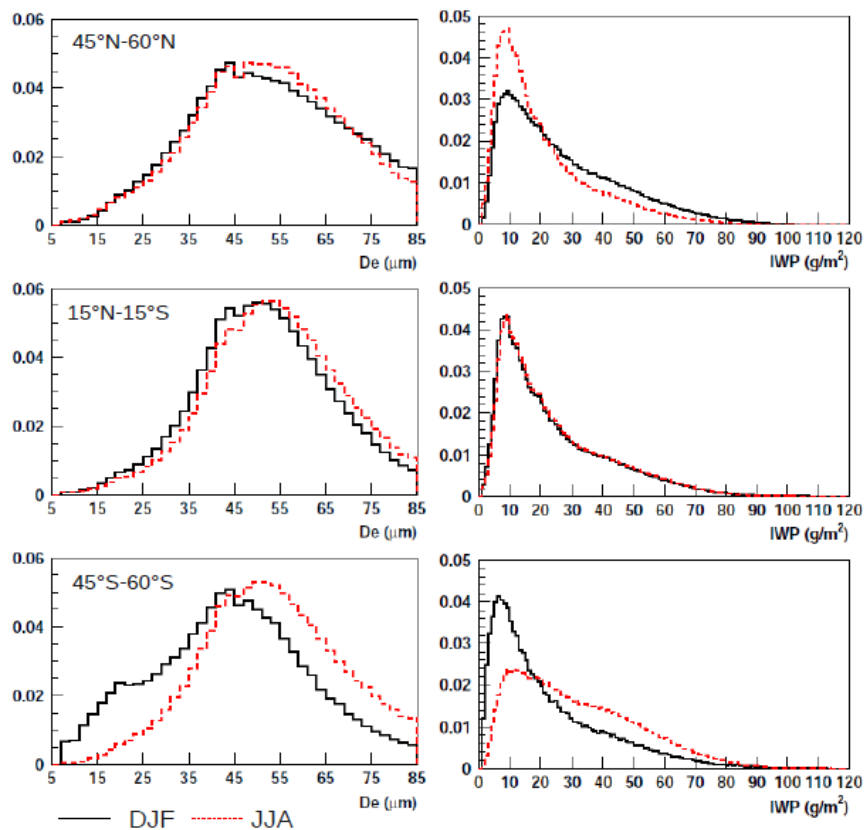
**Fig. 12.** Zonal distributions of ST-HIC microphysical properties from 2003 to 2009. $D_e$ distributions are presented on the left, IWP distributions on right, in three latitude bands (defined on the top left corner of the right side figures) and for boreal winter and boreal summer (full black lines and dashed red lines, respectively).

Title Page

Abstract | Introduction

Conclusions | References

Tables | Figures

|◄ | ►|

◄ | ►

Back | Close

Full Screen / Esc

Printer-friendly Version

Interactive Discussion
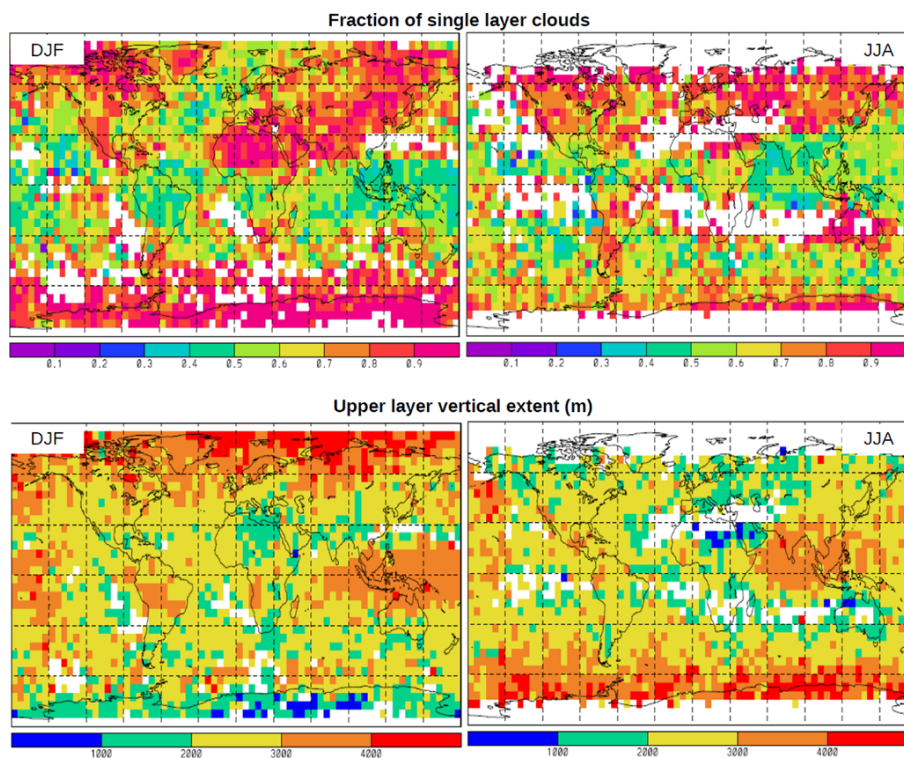
**Fig. 13.** Fraction of single layer clouds amongst the cirrus retrieved (on the top) and the vertical extent of their upper layer determined by the GEOPROF data (on the bottom), for boreal winter and boreal summer, respectively over 2007–2008.
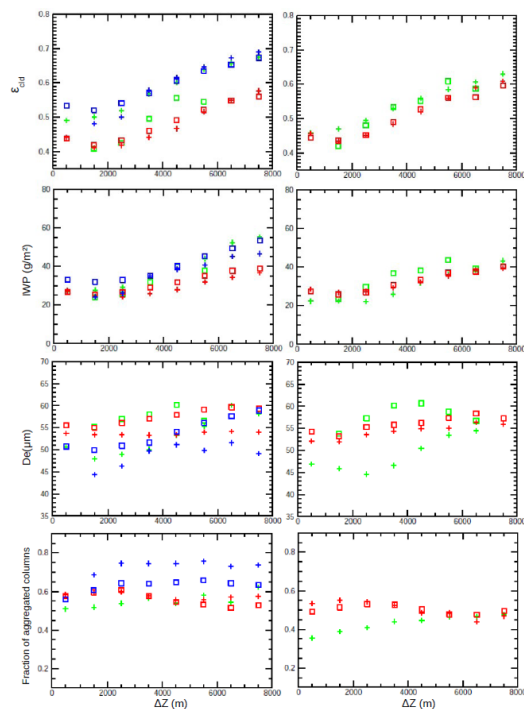
**Fig. 14.** Correlation between microphysical properties and geometrical depth from radar-lidar GEOPROF data separately over ocean and land on the left and right, separately. Green, red and blue signs stand for Northern Hemisphere, Tropics, and Southern Hemisphere, respectively. The plus sign and square are for DJF and JJA, respectively.
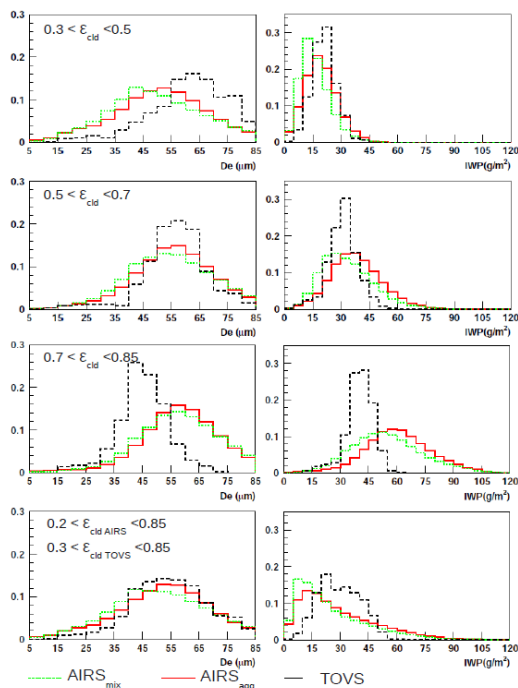
**Fig. 15.** Global annual microphysical properties' distributions for AIRS (aggregated-like and mixed shape, full red lines, and dotted green, respectively) and for TOVS (dashed black lines). $D_e$ distributions are presented in the left hand figures and IWP distributions in the right hand figures, for different optical thickness classes whose ranges are indicated on the top left hand corner of the figures in the left hand column.
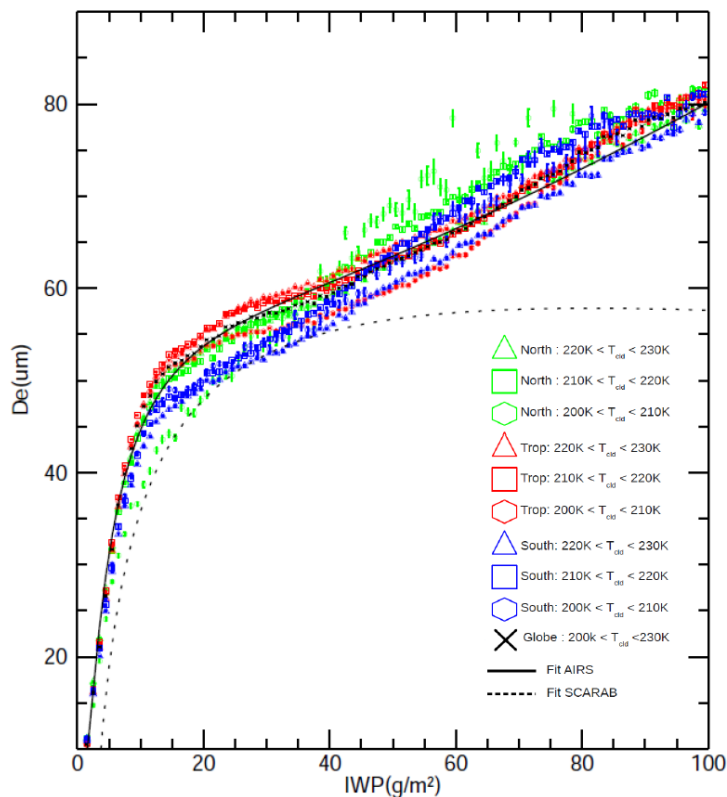
**Fig. 16.** Correlation between $D_e$ and IWP for mixed habits ice crystals over the period 2003–2009. Results are shown for different latitude bands and different temperature bins. The global correlation is also represented (black crosses) as well as its polynomial fit (black line).
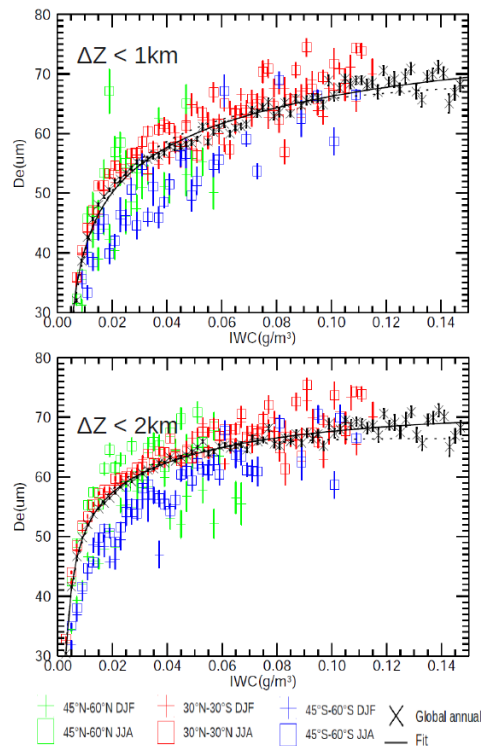
**Fig. 17.** Correlation between $D_e$ and an estimation of the average IWC for mixed habits ice crystals over the period 2003–2009. Results are shown for different latitude bands and different seasons. The global correlation is also represented (black crosses) as well as its polynomial fit (black line) and a fit using a parameterization developed in Mc Farquhar et al. (2003) (black dashed lines). The top figure is for clouds with a vertical extent lower than 1 km and the bottom figure is for clouds with a vertical extent lower than 2 km.

Title Page

Abstract | Introduction

Conclusions | References

Tables | Figures

|◄ | ►|

◄ | ►

Back | Close

Full Screen / Esc

Printer-friendly Version

Interactive Discussion